

Monsoon Climate Variabilities

Tim Li

*International Pacific Research Center and Department of Meteorology, School of Ocean and Earth Science and Technology
University of Hawai'i at Mānoa, Honolulu, Hawaii, USA*

The Asian monsoon consists of three subcomponents, Indian monsoon (IM), East Asian monsoon (EAM), and western North Pacific monsoon (WNPM). All these submonsoon systems exhibit remarkable intraseasonal and interannual variabilities. In this chapter, we will review recent progress in understanding the monsoon annual cycle and some of major issues related to the monsoon intraseasonal and interannual variabilities; describe the spatial-temporal structure of the northward propagating intraseasonal oscillation in the monsoon region; and discuss what physical processes lead to quasi-biennial and lower-frequency variabilities of the India monsoon, how El Niño (La Niña) events have a delayed impact on East Asian climate, and how the atmosphere-ocean interaction in the monsoon–warm ocean leads to the tropospheric biennial oscillation. Specific emphases are placed on the discussion of the physical processes that are responsible for the described phenomena.

1. INTRODUCTION

The Asian monsoon system consists of three subcomponents, Indian monsoon (IM), East Asian monsoon (EAM), and western North Pacific monsoon (WNPM). Plate 1a shows the domain of the three submonsoon systems [Wang *et al.*, 2003a] and the summer-winter difference of precipitation and low-level wind fields. As seen from the Plate 1a, the IM is characterized by lower level westerlies and upper level easterlies, being in a thermal wind relation with a north-south thermal contrast between the heated Asian land and cool Indian Ocean, while EAM has pronounced lower level southerlies in association with the east-west thermal contrast between the Asian continent and midlatitude Pacific Ocean [Zhu *et al.*, 1986; Tao and Chen, 1987]. Whereas IM and EAM are typical continental monsoons driven by land-ocean thermal contrast, WNPM is an oceanic monsoon driven primarily by hemispheric asymmetric sea

surface temperature (SST) gradients. Plate 1b shows climatological annual rainfall evolution averaged over the three equal-area boxes. The strength of the three submonsoon systems is distinctive, with greatest (least) total rainfall amounts occurring in the WNPM (EAM) region.

The time evolution of the Asian monsoon has distinctive regional characteristics (Plate 1c). The convection first develops over the Bay of Bengal (BOB) in late April. After that, the monsoon is triggered over the South China Sea (SCS) and then moves northward to East Asia. The EAM is normally referred to as a subtropical monsoon encompassing eastern China, Japan, Korea, and adjacent marginal seas and monsoon oceans, i.e., the area between 20° and 45°N and from 100° to 140°E [Chen and Chang, 1980; Tao and Chen, 1987; Zhang *et al.*, 1996]. The major rain-producing system is the monsoon subtropical front, which is also known as Meiyu or Baiu front during early summer when it is located along the Yangtze River Valley extending to southern Japan. The Meiyu is preceded by the onset of the SCS summer monsoon, which, on average, occurs in mid-May when heavy convective rainfall suddenly develops over the northern SCS and westerly flows control the central SCS [e.g., Wang and Wu, 1997;

Xie *et al.*, 1998; Lau and Wu, 2001]. The SCS onset is first followed by an establishment of a rainband over the northwest flank of the western North Pacific (WNP) subtropical high extending from the southern coast of China and Taiwan to east of Okinawa [Johnson *et al.*, 1993; Tanaka, 1997; Wang and LinHo, 2002]. Around 10 June, the EAM front and associated rainband move rapidly northward to the Yangtze River Valley and southern Japan, where continuous rain and cloudiness last for about a month. In mid-July the rain belt further advances northward to northern and northeast China [Tao and Chen, 1987; Ding, 1992, 1994]. In late August, the EAM begins to withdraw southward in northern China. The subseasonal stepwise progression of the EAM rainband [Lau *et al.*, 1988] is one of the features distinctive from the IM. During the IM period, the convective rainband gradually moves northward from the BOB and Arabian Sea from early May to July. The WNPM, on the other hand, is characterized by the eastward propagation of convective rainbands from middle May to August [Wu and Wang, 2001].

In the Asian monsoon region, there exist remarkable intraseasonal oscillation (ISO) signals in rainfall and circulation fields. ISO was first detected by Madden and Julian [1971], who found a significant period of 40–50 days in the zonal wind field over the Canton Island. Later they documented further the spatial structure of the ISO [Madden and Julian, 1972] and found that this oscillation is of global scale and is characterized primarily by equatorial eastward propagation with a zonal wave number–one structure. While the eastward propagating ISO mode is primarily observed in boreal winter, the ISO in boreal summer is dominated by northward propagation in the Asian monsoon region [e.g., Yasunari, 1979, 1980; Sikka and Gadgil, 1980; Krishnamurti and Subrahmanyam, 1982; Murakami *et al.*, 1984; Lorenc, 1984; Cadet, 1986; Lau and Chan, 1986; Wang and Rui, 1990]. For example, Krishnamurti and Subrahmanyam [1982] noted a steady meridional propagation of a train of troughs and ridges that form near the equator and dissipate near the foot of Himalayas over the Indian subcontinent sector. The meridional length scale of this mode is about 3000 km, and its meridional phase speed is about 0.75° latitude per day. By analyzing the 1975–1985 pentad mean outgoing longwave radiation (OLR) data, Wang and Rui [1990] classified the ISO events into three categories: eastward propagation (65%), independent northward propagation (20%), and westward propagation (15%). The eastward propagation mode trapped near the equator is more active in boreal winter than in summer. The northward propagation is found over Indian and western Pacific monsoon regions, while the westward propagation is mainly

confined in the off-equatorial western Pacific from May to October.

Plate 2 illustrates the total variance of the boreal summer ISO (BSISO) over a 20 year period and area-averaged rainfall evolution over the India monsoon region (15° – 30° N, 60° – 100° E) in 2004. Note that the amplitude of the intraseasonal rainfall variation over the region is comparable to that of the annual cycle and that the intraseasonal variation is closely linked to the northward propagation of the ISO convection over the BOB. Given that this most striking northward propagating feature of BSISO is completely missed in many of the current state-of-the-art general circulation models (GCMs) [Waliser *et al.*, 2003], a fundamental question that needs to be addressed is, What causes the northward propagation of the BSISO convection in the monsoon region?

Besides the intraseasonal variability, the monsoon also shows significant year-to-year changes. Among many factors, the El Niño–Southern Oscillation (ENSO) has been considered as a major factor that affects the IM rainfall variability. Walker [1923, 1924] first recognized the effect of the Southern Oscillation on IM. Since then, a number of studies have been conducted to elucidate the monsoon–ENSO relationship [e.g., Yasunari, 1990; Webster and Yang, 1992; Ju and Slingo, 1995; Lau and Yang, 1996] (see Webster *et al.* [1998] for a review). The IM tends to have a simultaneous negative correlation with the eastern Pacific SST [e.g., Rasmusson and Carpenter, 1983], although this simultaneous negative correlation has been broken in the two recent decades [Kumar *et al.*, 1999; Chang *et al.*, 2001].

The power spectrum of the time series of the domain-averaged India rainfall reveals that on interannual time scales there are two distinctive peaks (Figure 1), with the quasi-biennial (QB) component (2–3 years) (hereinafter referred to as the monsoon QB mode or tropospheric biennial oscillation (TBO) mode) being much greater than the lower-frequency (LF) component (3–7 years) (hereinafter referred to as the monsoon LF mode). Two similar power spectrum peaks also appeared in the global precipitation field [Lau and Sheu, 1988; Zhou *et al.*, 2008], the East Asian summer monsoon [Zhou and Yu, 2005], the meridional wind over the South China Sea, and sea level pressure difference between the Asian continent and northwestern Pacific [Tomita and Yasunari, 1996]. Webster *et al.* [1998] investigated the temporal characteristics of the Indian monsoon rainfall variability by use of a wavelet analysis and found the intermittent recurrence of the two power spectrum peaks. The Niño 3.4 SST anomaly (SSTA) also has two significant spectrum peaks, but its LF component is much greater than its QB component. Natural questions that need to be addressed are why the Indian monsoon has a more

pronounced QB spectrum peak and what physical mechanisms are responsible for the monsoon variability on both the time scales.

While the IM is primarily influenced by ENSO during its developing phase, the interannual variability of EAM is highly correlated with ENSO during its decaying phase. In

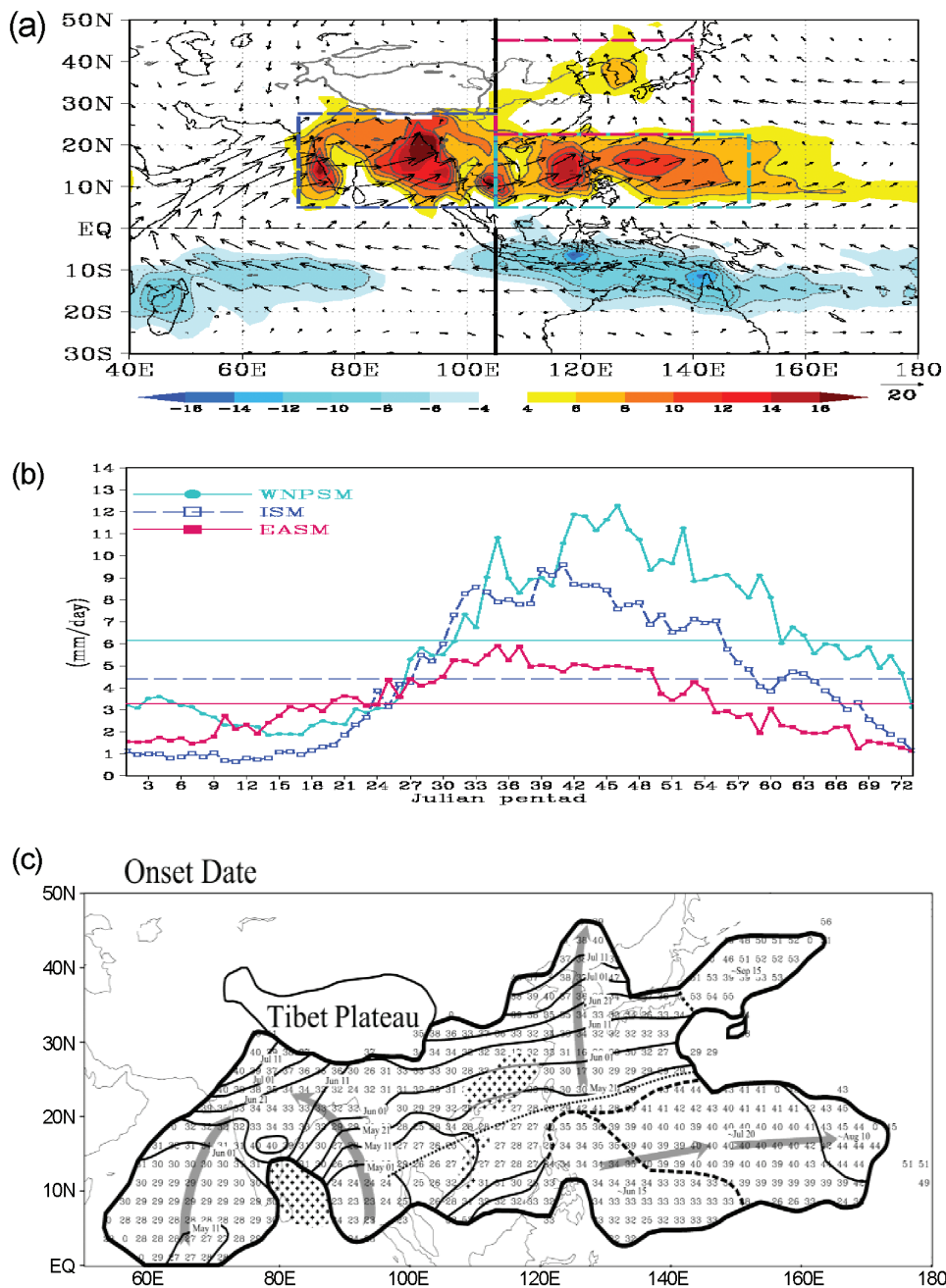


Plate 1. (a) Domain of IM, WNPM, and EAM and rainfall (shading) and 850 hPa wind (vector) difference fields between July–August and January–February. (b) Climatological pentad rainfall evolution averaged over the IM, WNPM, and EAM boxes. Reprinted from *Wang et al.* [2003a] with permission from Elsevier. In Plate 1b, ISM, EASM, and WNPSM denote averaged rainfall over Indian, East Asian, and WNP summer boxes. (c) Climatological onset date for the Asian monsoon region [from *Wang and Lin*, 2002]. © Copyright American Meteorological Society.

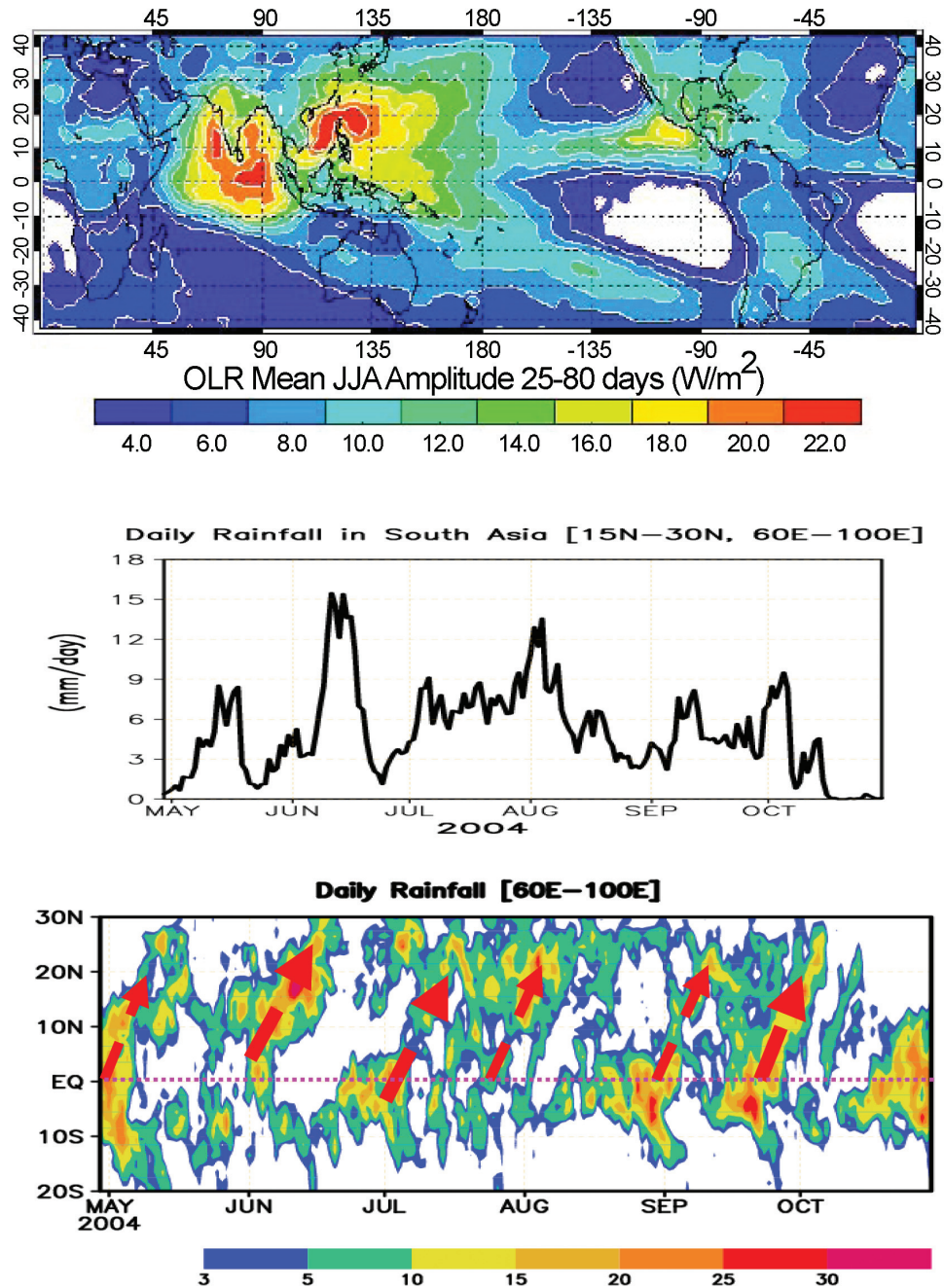


Plate 2. (top) Standard deviation of 25–80 day filtered outgoing longwave radiation (OLR) fields for the period of 1981–2002. (middle) Time evolution of 2004 daily rainfall averaged over South Asia (15° – 30° N, 60° – 100° E). (bottom) Latitude-time section of the 2004 daily rainfall averaged along 60° – 100° E.

the summer after an El Niño, the Meiyu/Baiu rainfall tends to be abundant [Zhang *et al.*, 1996; Lau and Yang, 1996; Yeh and Huang, 1996; Kawamura, 1998; Chang *et al.*, 2000a, 2000b], even though during that season, SST in the eastern equatorial Pacific is nearly normal (Figure 2). The

physical mechanism behind this delayed impact of ENSO on the EAM needs to be understood.

To sum up, in this chapter we intend to address the following scientific questions that are related to the monsoon intraseasonal and interannual variabilities:

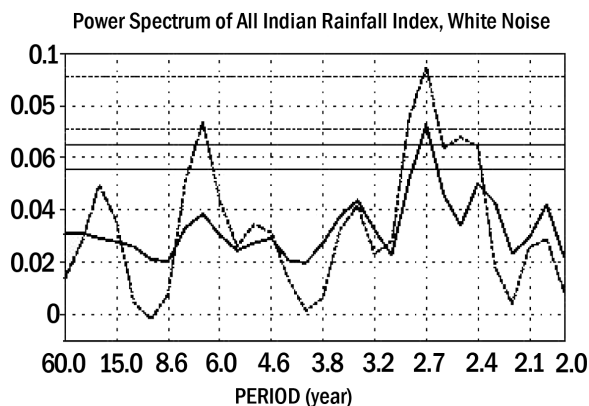


Figure 1. Power spectra of the domain-averaged Indian rainfall time series for the period of 1949–1998. The dashed line shows the 95% significance level.

1. What is the characteristic spatial structure of the northward propagating BSISO? What is the physical mechanism responsible for the northward propagation?
2. What are the specific processes that determine the QB and LF variabilities of the Indian monsoon?
3. How does the El Niño affect the IM and EAM? Why does the influence of ENSO differ in its developing and decaying years? In particular, why does ENSO have a delayed impact in the summer after the ENSO peak when the El Niño disappears?
4. Why does the monsoon have a strong biennial tendency? What is the specific air-sea interaction process in the warm ocean that causes the TBO?

These questions will be discussed sequentially in sections 2 through 5.

2. STRUCTURES AND MECHANISMS OF THE NORTHWARD PROPAGATION OF BSISO

Several mechanisms were proposed to understand the northward propagation of the BSISO. For example, *Webster* [1983] hypothesized that the land surface heat flux into the atmospheric planetary boundary layer (PBL) may play a role in destabilizing the atmosphere ahead of the convection, leading to a northward shift of the convective zone. However, the strongest observed northward propagating signal appears over the ocean not over the land. On the basis of simulations from an intermediate atmospheric model, *Wang and Xie* [1997] proposed a Rossby wave emanation hypothesis. As the convection moves eastward to the central equatorial Pacific, the reduction of the mean SST and specific humidity leads to the emanation of Rossby waves from the equatorial convection, which forms a “convection front.” This “convection front” tilts northwestward from the equator to 20°N (a V shape), resulting in an apparent northward movement as the entire wave packet migrates eastward. This Rossby wave emanation hypothesis was supported by *Lawrence and Webster* [2002], who showed that a large portion of the northward propagation is connected to the eastward moving component in their wave number–frequency analysis maps. The air-sea interaction is another possible mechanism, because reduced surface latent heat fluxes (due to a decrease in the total

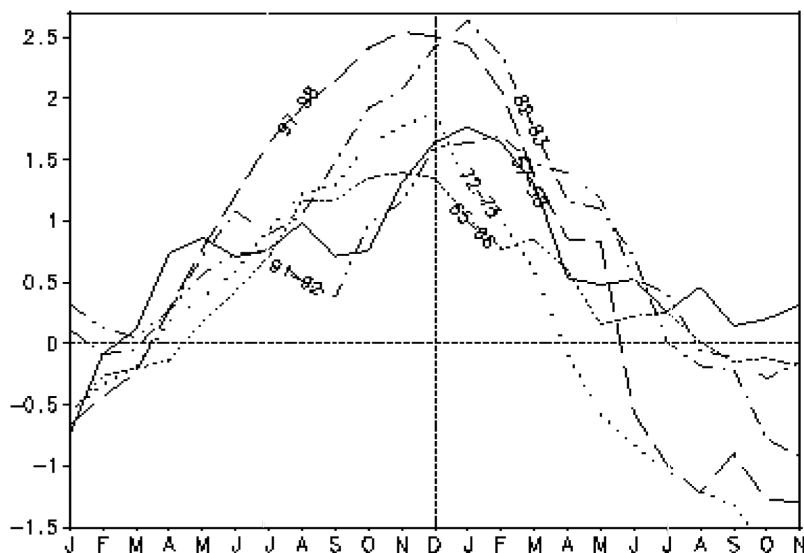


Figure 2. Time evolution of Niño 3.4 SSTA for individual El Niño events in the past 50 years.

wind speed) may increase SST to the north of the convection, leading to a moisture convergence in the PBL [Kemball-Cook and Wang, 2001]. Thus, the atmosphere north of the convection is destabilized, and the convection moves northward. It is unclear whether the resulting SSTA plays an active role in the northward propagation or it is simply a passive response to the atmospheric forcing.

To reveal essential atmospheric dynamical processes that give rise to the northward propagation of the BSISO, Jiang *et al.* [2004] conducted a diagnostic study by analyzing both the observations (National Centers for Environmental Prediction (NCEP) reanalysis) and atmospheric general circulation model (AGCM) simulations. The reason for analyzing both data sets is that the AGCM simulations exclude the effect of air-sea interactions as the model specifies climatological monthly mean SST. By comparing the two analyses, one may identify what part of BSISO structures are attributed to atmospheric process only and what part may be due to effect of atmosphere-ocean interactions.

The model used in this study is the European Centre/Hamburg (ECHAM) AGCM version 4.0 [Roeckner *et al.*, 1996] at a resolution of T30 (spectrum truncation to 30 wave numbers) and 19 vertical levels. The convection scheme used in this AGCM is the mass flux scheme for penetrative, shallow, and mid-level convection [Tiedtke, 1989], modified by Nordeng [1996] so that the cloud base mass flux is linked to convective instability for the penetrative convection. This model is integrated for 15 years, with the lower boundary condition given by the climatological monthly mean SST. Daily averaged fields are written out for analysis.

The daily NCEP–National Center for Atmospheric Research (NCAR) reanalysis data set for the period from 1980 to 2001 is used. The horizontal resolution of the reanalysis data is 2.5° longitude by 2.5° latitude, and vertically there are 12 pressure levels. The 3-D variables include the zonal and meridional wind components, vertical p velocity, and specific humidity. The NOAA daily averaged OLR data are employed as the proxy for convection. To compare the model precipitation with the observed, the Climate Prediction Center (CPC) Merged Analysis of Precipitation (CMAP) data [Xie and Arkin, 1997] are used. A band-pass-filtering method is applied to isolate the ISO signal. For daily data, harmonics between 4 and 24 are extracted each year, which corresponds to the period of 15–90 days. This time filtering is applied to each meteorological field for both the model output and the NCEP-NCAR reanalysis.

2.1. BSISO Meridional-Vertical Structures

The ECHAM AGCM is integrated for 15 years with specified climatological monthly SST. The model reproduces

the gross pattern of mean precipitation and the northward propagation of the ISO, the latter may be identified by a Hovmöller diagram of the rainfall along 70° – 95° E. Note that the northward propagation is most pronounced during the boreal summer each year. To reveal the meridional and vertical structure of the BSISO, we take a composite approach by selecting 23 strong northward propagation cases. The composite is constructed such that at day 0 the ISO convection arrives exactly at 5° N along 70° – 95° E. The time sequence of the composite rainfall from day -16 to 12 shows that an ISO convection center is located in the equatorial western Indian Ocean (about 60° E) at day -16 and the intensity of the convection is weak. In the ensuing days, the convection intensifies and moves eastward along the equator. At day -8 , the maximum rainfall center arrives in the eastern equatorial Indian Ocean around 90° E. After that, the convection starts to move northward, and at the same time it intensifies. At day 4, the convection arrives at 10° N and reaches the maximum intensity. Later it begins to weaken while continuing to move northward. At day 10, the convection center arrives in the northern BOB. The meridional phase speed of the BSISO may be estimated from the time-latitude section of the composite rainfall (based on the axis of the maximum rainfall). The average propagation speed from the equator to 20° N is about 1.0° of latitude per day.

The same analysis approach is applied to the daily NCEP/NCAR reanalysis data. Here the negative OLR is used to represent the convection and a total of 25 strong northward propagation cases are selected. The following BSISO features derived from the model are confirmed by the observational data. (1) A new convection is initiated over the western equatorial Indian Ocean, which then moves to the eastern equatorial Indian Ocean along the equator. (2) After moving to the eastern equatorial Indian Ocean around 90° E, the convection begins to move northward toward the northern Bay of Bengal. (3) No clear evidence shows the connection between the northward propagation of the ISO convection over the Indian Ocean and the eastward propagation in the western equatorial Pacific Ocean. The meridional phase speed along 75° – 90° E may be calculated on the basis of the latitude-time profile of the observed OLR field. The result shows that an average northward propagation speed is 0.93° of latitude per day, similar to that obtained from the AGCM.

Next we examine the meridional phase relationship among various meteorological fields associated with the northward propagating BSISO mode in an attempt to unveil fundamental dynamics behind the northward propagation. We pay special attention to the meridional asymmetry of dynamic and thermodynamic fields with respect to the convection center. The BSISO mode structure is composed on the basis of the most significant northward propagation

cases. We first construct the phase structure at each reference latitude over which the maximum convection occurs. As these phase structures bear great similarity, we further compose them with respect to the maximum convection center for different latitudes.

Figure 3 shows the meridional-vertical structure of the composite BSISO mode from NCEP reanalysis. To clearly

illustrate the meridional phase relationship, we have applied a cubic-spline interpolation for each field in the meridional direction. From Figure 3, one can see that maximum vertical motion occurs in the middle troposphere (about 400 hPa) and coincides with the convection center. Associated with this maximum ascending motion are the low-level convergence and the upper tropospheric divergence.

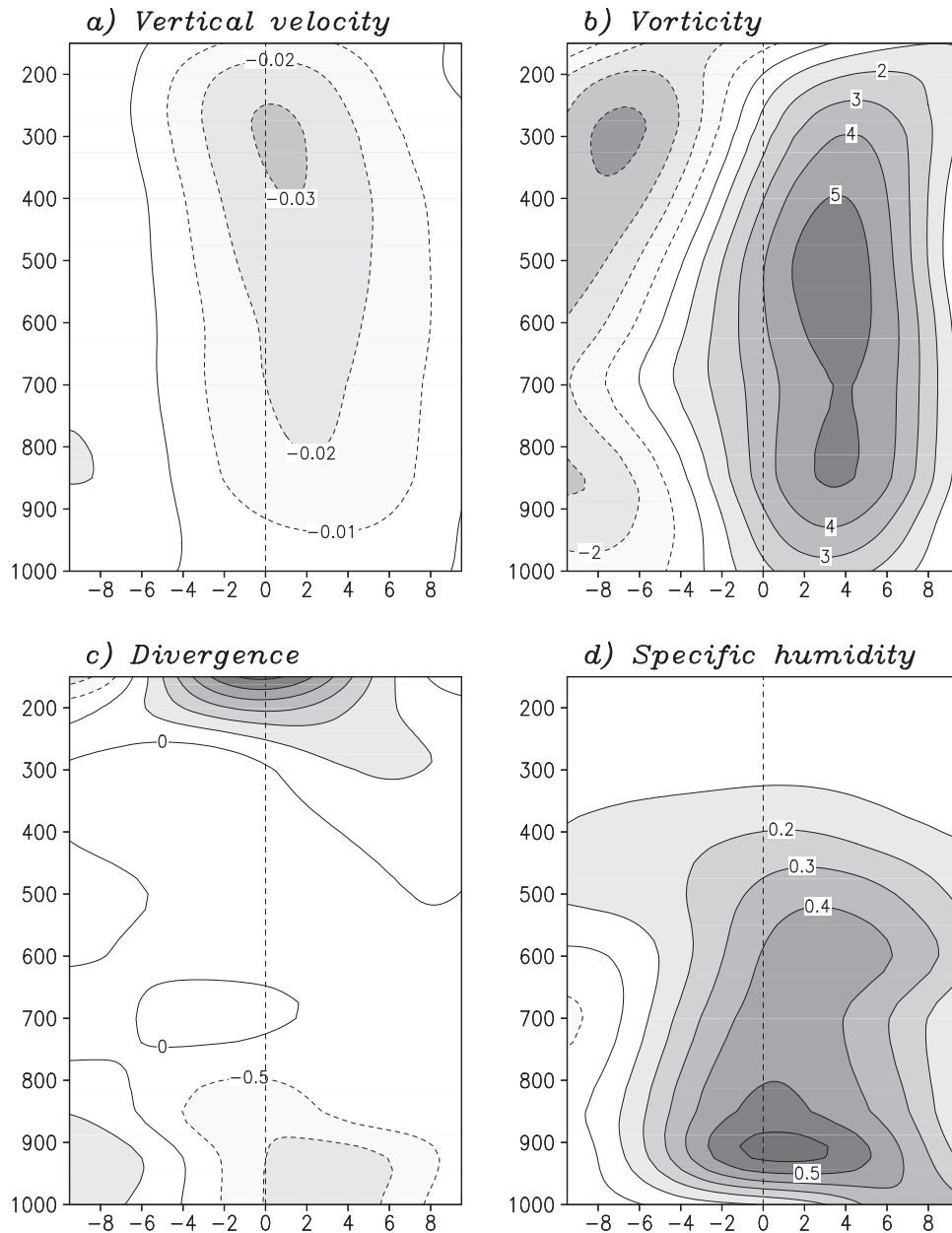


Figure 3. (a) Composite meridional-vertical structure of the p vertical motion (unit: Pa s⁻¹), (b) vorticity (unit: 0.00001 s⁻¹), (c) divergence (unit: 0.00001 s⁻¹), and (d) specific humidity (unit: g kg⁻¹) fields of the northward propagating BSISO mode derived from NCEP reanalysis fields during 1980–2001.

The most striking asymmetric structure with respect to the convection center appears in the vorticity field. A positive vorticity center with an equivalent barotropic structure is located 400 km north of the convection center, while a negative vorticity with the same equivalent barotropic structure appears to the south of the convection center. Another striking asymmetry appears in the specific humidity field. A maximum specific humidity center shifts about 150 km to the north of the convection center in the lower troposphere. The temperature and geopotential height fields also show a significant phase difference relative to the convection.

The asymmetric feature of vorticity and humidity with respect to the BSISO convection center is well reproduced by the model. The resemblance of the model and observed BSISO structure and propagation characteristics suggests that to the first order of approximation, it is the internal atmospheric dynamics that are essential to cause the northward propagation.

A distinctive feature, compared to the model, lies in the low-level divergence and vertical velocity fields. In the NCEP/NCAR reanalysis data, the PBL convergence tends to lead the convection by 3°. This is accompanied by the tilting of the maximum vertical velocity axis. While the vertical motion in the middle troposphere is in phase with the convection, it shifts to the north at the lower levels. It is likely that this northward shift of the PBL convergence results from the Ekman pumping induced by the positive vorticity at the top of the PBL ahead of the convection. The model, however, fails to capture this feature, possibly because of too strong turbulent mixing in the lower troposphere. This is partly reflected by the height of the maximum specific humidity center. While the observed maximum specific humidity center is confined in the boundary layer below 850 hPa, the model specific humidity peaks in a much higher altitude (around 650 hPa).

2.2. Mechanisms for the Northward Propagation

On the basis of meridional and vertical structures illustrated above, the following two internal atmospheric dynamical mechanisms are unveiled to explain the northward propagation of the BSISO.

2.2.1. Vertical shear mechanism. This mechanism is evidenced by the observed and modeled BSISO structure of an equivalent barotropic vorticity field that appears to the north of the convection center. In the following, by using a 2.5-layer intermediate atmospheric model, we demonstrate how the vertical shear of the summer mean flow leads to the coupling of barotropic and baroclinic modes and the development of a meridionally asymmetric barotropic vorticity field.

For demonstration purposes, a 2.5-layer model is used here, following *Wang and Li* [1993, 1994]. The model consists of a two-layer free atmosphere and a well-mixed PBL. For simplicity, we consider a 2-D case with vanished zonal gradients for all variables. The governing equation for a linear motion in an f plane under a constant vertical shear of the mean zonal flow can be written as

$$\frac{\partial \zeta_-}{\partial t} + f_0 D_- = -\bar{u}_T \frac{\partial D_+}{\partial y} + K \cdot \nabla^2 \zeta_-, \quad (1)$$

$$\frac{\partial D_-}{\partial t} - f_0 \zeta_- + \nabla^2 \phi_- = K \cdot \nabla^2 D_-, \quad (2)$$

$$\frac{\partial \zeta_+}{\partial t} + f_0 D_+ = 2\bar{u}_T \frac{\partial}{\partial y} (2D_+ + D_-) + K \cdot \nabla^2 \zeta_+, \quad (3)$$

$$\frac{\partial D_+}{\partial t} - f_0 \zeta_+ + \nabla^2 \phi_+ = K \cdot \nabla^2 D_+, \quad (4)$$

$$\frac{\partial \phi_-}{\partial t} - f_0 \bar{u}_T v_+ + c_0^2 (1-I) D_- = c_0^2 (B-1) D_+ + K \cdot \nabla^2 \phi_-, \quad (5)$$

where t denotes time, y denotes meridional distance, ζ is relative vorticity, D is divergence, ϕ is geopotential height, $\bar{u}_T = \frac{\bar{u}_1 - \bar{u}_3}{2}$ denotes the constant vertical shear of the mean flow, K is the diffusion coefficient, f_0 is the Coriolis parameter at a reference latitude (12°N), c_0 is the gravity wave speed of the free-troposphere baroclinic mode, I is the heating coefficient associated with wave convergence, and B is the heating coefficient associated with frictional convergence. Variables with a plus (minus) subscript represent a barotropic (baroclinic) mode. For the detailed derivation of the governing equations and the description of major parameters and their values in the equations, readers are referred to *Jiang et al.* [2004]. The purpose of using an f plane is to exclude the Rossby wave emanation mechanism [*Wang and Xie*, 1997; *Lawrence and Webster*, 2002] so that one can focus on the effect of the basic state vertical shear.

The motion in the PBL is controlled by the geopotential height at the top of the boundary layer, which is assumed to be equal to the geopotential height in the lower troposphere [*Wang and Li*, 1993]. Thus, we have

$$E u_B - f_0 v_B = 0, \quad (6)$$

$$E v_B + f_0 u_B = -\frac{\partial(\phi_+ - \phi_-)}{\partial y}. \quad (7)$$

Equations (6) and (7) lead to

$$\frac{-E}{E^2 + f_0^2} \frac{\partial^2(\phi_+ - \phi_-)}{\partial y^2} = \frac{\partial v_B}{\partial y} = \frac{w_B}{p_s - p_e} = -\frac{2\Delta p}{p_s - p_e} D_+, \quad (8)$$

humidity with respect to the convection. Mathematically, this process may be expressed as

$$\frac{\partial q}{\partial t} \propto -\bar{v}_B \frac{\partial q}{\partial y} - w_B \frac{\partial \bar{q}}{\partial p}$$

where q is specific humidity and p is pressure.

Physically, it is interpreted as follows. Consider a strong ISO convection with a convergence at the surface level and a divergence at the upper level. The convergence at the surface level will induce the upward motion in the atmospheric boundary layer, which will bring the rich moisture at the surface to a certain level in the lower troposphere. The advection effect by the summer mean meridional wind in the PBL may further shift the specific humidity center to the north of the convection. As the convective heating largely depends on the moisture convergence, the shifted moisture center will lead to the northward displacement of the convective heating and thus the convection tends to move northward.

Another possible process that leads to the northward shift of the moisture is through the advection effect by the ISO wind in the presence of the mean meridional specific humidity gradient [*Li and Wang, 1994*]. The meridional distribution of JJA surface specific humidity averaged over the Indian subcontinent sector shows that the maximum moisture is located around 20°N over the northern Indian Ocean. To the south of 20°N, the meridional gradient of the mean specific humidity is positive. Considering the advection by the ISO wind, the moisture equation may be written as

$$\frac{\partial q}{\partial t} \propto -v_B \frac{\partial \bar{q}}{\partial y}$$

In response to the ISO convective heating, the perturbation wind has a southward flow to the north of and a northward flow to the south of the convection center. As a result, the moist perturbation has an asymmetric structure, with a positive center appearing to the north of the convection center and a negative center appearing to the south of the convection.

This moisture-convection feedback mechanism works for all latitudes from 10°S to 20°N (including the equatorial region), providing valuable additions to the vertical shear mechanism for explaining the observed northward propagation feature.

An eigenvalue analysis is further conducted in a model that includes the effect of the vertical shear, moisture-convection feedback, and atmosphere-ocean interactions [*Jiang et al., 2004*]. It is noted that the northward propagating BSISO mode is an unstable mode of the summer mean flow in the monsoon region. The analysis result also

points out the relative importance of various processes in contributing to the northward propagation. While the vertical shear plays an important role away from the equator in the Northern Hemisphere, the moisture-convection feedback and air-sea interaction also contribute significantly, particularly in the region near and south of the equator. Overall, given the similar structure and propagation characteristics of the BSISO in the model and the observation, it is concluded that it is the internal atmospheric dynamics that are essential to give rise to the northward propagation over the tropical Indian Ocean.

3. PROCESSES DETERMINING THE QB AND LF VARIABILITY OF THE INDIAN MONSOON

In this section we discuss the physical mechanisms responsible for the quasi-biennial and low-frequency variability of the Indian monsoon rainfall by revealing the spatial and temporal structures of atmospheric circulation and SST associated with the monsoon TBO and LF modes. Our strategy is first to apply a time-filtering technique to separate rainfall data into 2–3 year and 3–7 year bands, respectively. Then, by analyzing the spatial and temporal patterns of atmospheric circulation associated with the two bands, we intend to investigate physical processes responsible for the rainfall variability on the two time scales.

The primary data used in this study are the domain-averaged Indian rainfall, NCAR/NCEP reanalysis that includes wind, moisture, temperature and geopotential height fields, and the Reynolds SST [*Reynolds and Smith, 1994*] for the period of 1949–1998. The Indian rainfall is represented by an area-averaged precipitation from 26 stations reasonably distributed over the Indian subcontinent. These gauge stations are picked up from the NOAA climatological baseline station data. The area-averaged rainfall has a correlation coefficient of 0.86 with the all-Indian-rainfall index [*Mooley and Parthasarathy, 1984*].

A band-pass filter [*Murakami, 1979*] is used to separate the data into approximately 2–3 year and 3–7 year windows, respectively. These two bands represent the two significant power spectrum peaks in the area-averaged Indian rainfall field. A lagged correlation analysis is then performed for each data set. A composite analysis using the original unfiltered data is also carried out to cross-check the lagged correlation analysis results obtained from the time-filtered data. For more detailed description of the data and analysis methods, readers are referred to *Li and Zhang [2002]*.

Plate 3 shows the lagged correlations between the Indian summer rainfall and SST anomalies in the tropical Indian

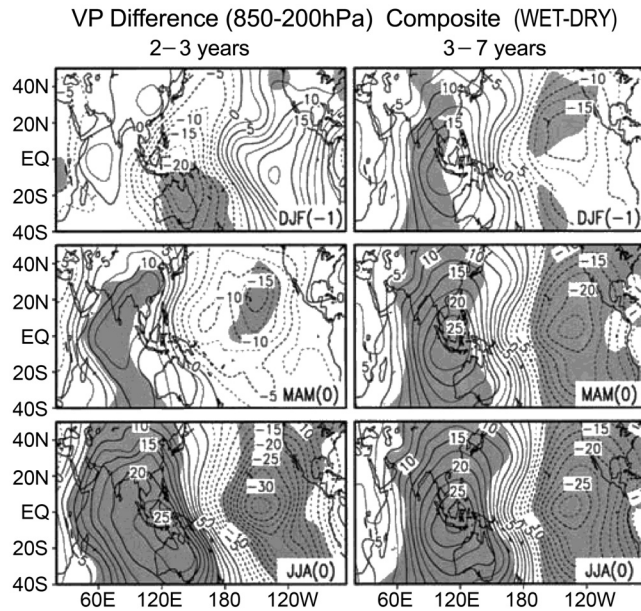


Figure 5. Wet-minus-dry composites of the velocity potential (VP) difference (850 hPa minus 200 hPa) field (counter interval: $2.5 \times 10^5 \text{ m}^2 \text{ s}^{-1}$) in December-January-February (DJF)(-1), March-April-May (MAM)(0), and June-July-August (JJA)(0) for the 2–3 year and 3–7 year bands. The shaded regions represent the statistical significance of 95% and above.

ocean warming through (1) reduced surface evaporation (because the mean wind is northerly in northern winter) and (2) anomalous meridional temperature advection that brings warmer water from the south. Thus, on the TBO time scale a strong Indian summer monsoon is preceded by a weak winter Asian monsoon that is characterized by anomalous southerly wind over the northern IO.

Another notable feature associated with the monsoon TBO mode is the phase reversal of the eastern Pacific (EP) SSTA in spring. The SST correlation coefficient changes its sign from a positive value in the preceding winter to a negative value in summer. Associated with this SSTA phase transition, the surface wind anomaly switches from westerly to easterly in the central equatorial Pacific.

In contrast to their high lagged correlation, the simultaneous correlation between the Indian monsoon and the IO SSTA is very low. This is because a strong Indian monsoon generates strong surface winds that further cool the ocean through enhanced surface evaporation and ocean mixing. As a result, the SSTA weakens rapidly in summer in the northern IO, especially along the eastern coast of Africa and in the Arabian Sea.

For the monsoon LF mode, the most significant SST correlation appears in the Pacific. While the western Pacific (WP) SSTA has a positive, lagged correlation (+0.4)

with the monsoon in the preceding winter, the EP SSTA has a simultaneous negative correlation (–0.5). The correlation with the IO SSTA is weak for all seasons prior to the monsoon onset, whereas a negative correlation appears after the monsoon onset, indicating a possible monsoon impact on the IO SSTA.

A common feature in both the 2–3 year and 3–7 year bands is that there is a strong simultaneous, negative correlation between the Indian monsoon and the EP SSTA. This points out an interactive nature of the monsoon-ENSO system. On one hand, a positive (negative) SSTA may have a remote impact on the monsoon through large-scale vertical overturning [Meehl, 1987]. On the other hand, anomalous monsoon heating may alter the EP SST through the change of winds over the central and western Pacific [Chang and Li, 2001].

To examine the effect of anomalous moisture transport, we composite the 1000 hPa moisture flux convergence field on the basis of the NCEP/NCAR reanalysis data. The 10

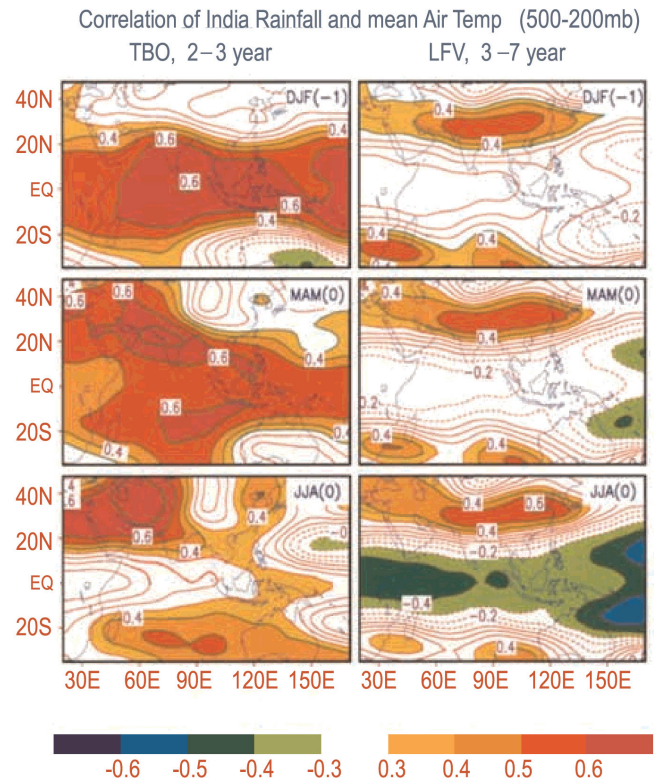


Plate 4. Lagged correlation maps between the all-India monsoon rainfall and the mean tropospheric (200–500 hPa) temperature in DJF(-1), MAM(0), and JJA(0) for the 2–3 year and 3–7 year bands (contour interval: 0.1). The regions where the positive or negative correlation exceeds 0.3 are shaded. The statistical significance exceeds the 95% level when the correlation is above 0.4.

wettest and 10 driest years are selected on the basis of the filtered monsoon rainfall data for both bands. From wet-minus-dry composites, one can see that in the 2–3 year band, there is a significant low-level moisture convergence over the Indian subcontinent in the preceding winter and spring. In the 3–7 year band, the anomalous moisture flux convergence is quite different: no significant moisture convergence appears in the Indian subcontinent.

The Walker circulation is regarded as an important agent that links the Pacific Ocean to the Asian monsoon. Since the vertical motion in the midtroposphere is related to upper and lower tropospheric divergent flows, we use the velocity potential difference (VPD) between 850 hPa and 200 hPa to represent the vertical overturning cell of the Walker circulation. A positive (negative) VPD center corresponds to a strong ascending (descending) motion. Figure 5 illustrates the composite VPD field for the 2–3 year and 3–7 year bands. A similar feature in both bands is that in summer (June–July–August (JJA)), the Walker circulation is characterized by a strong ascending (descending) branch over the monsoon (EP) region. However, the evolution of the Walker cell in the two bands is quite different. For the LF mode (Figure 5,

right), the ascending and descending branches are almost stationary, whereas for the QB mode (Figure 5, left) there is slow eastward propagation of the ascending and descending branches. This temporal evolution feature is somewhat similar to that found by *Barnett* [1991]. Another feature in the 2–3 year band is that even though there is a remote SSTA forcing in the EP in winter, an ascending branch appears in the equatorial IO. This ascending motion results from the direct impact of the warm SSTA in the IO, which compensates for the effect of the El Niño in the EP. Thus, in addition to its moisture effect, the IO SSTA may have a dynamic impact on the vertical overturning of the Walker cell.

The land-ocean thermal contrast between the Asian continent and Indian Ocean was regarded as an indication of the monsoon strength [e.g., *Li and Yanai*, 1996; *Yang et al.*, 1996]. To examine the role of the land-ocean thermal contrast on the monsoon variability, we calculated the lagged correlation between the monsoon rainfall and the mean (between 200 and 500 hPa) tropospheric temperature. Plate 4 shows the lagged correlation maps. At the 2–3 year window (Plate 4, left), the increase of the tropospheric mean temperature is concurrent with the warming of the

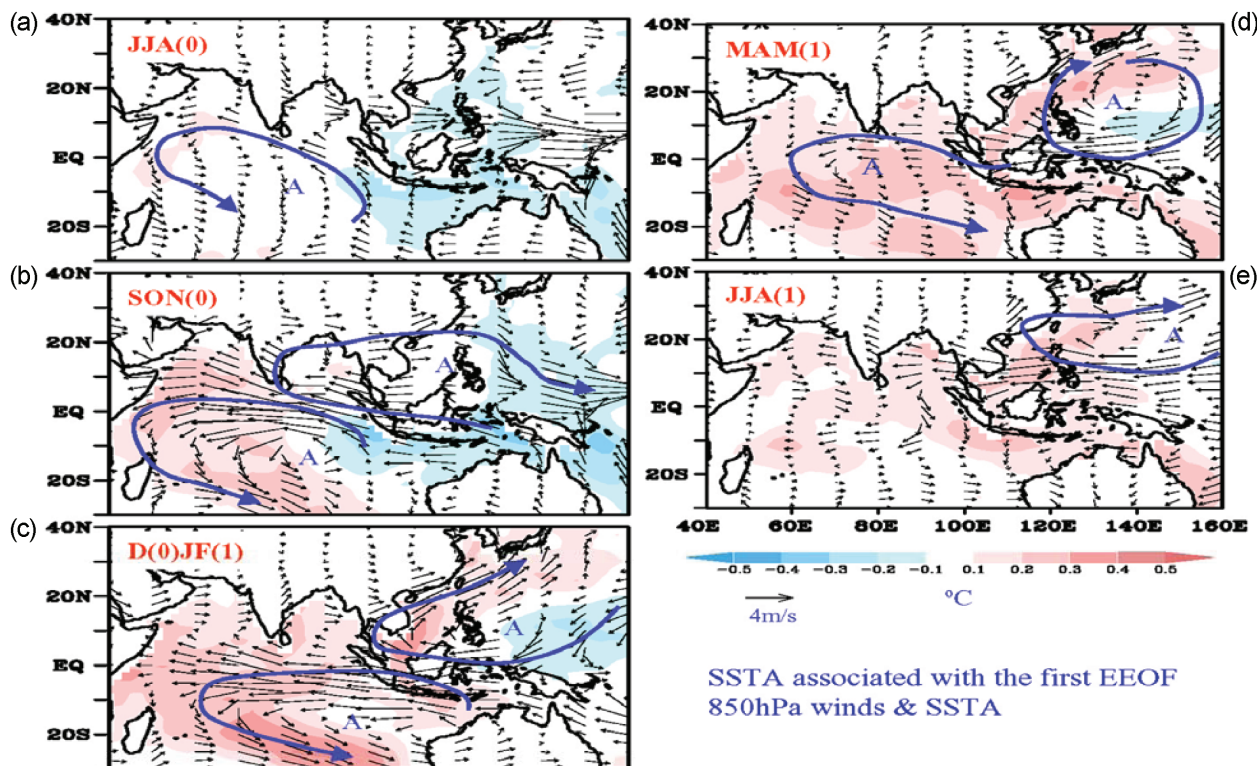


Plate 5. Seasonal evolving patterns of 850 hPa wind (vectors) and SST (shading) anomalies associated with El Niño turnabout from the developing summer, JJA(0), to the decaying summer, JJA(1), (a) JJA(0), (b) SON(0), (c) D(0)JF(1), (d) MAM(1), and (e) JJA(1), calculated on the basis of the SS-SVD analysis [from *Wang et al.*, 2003b].

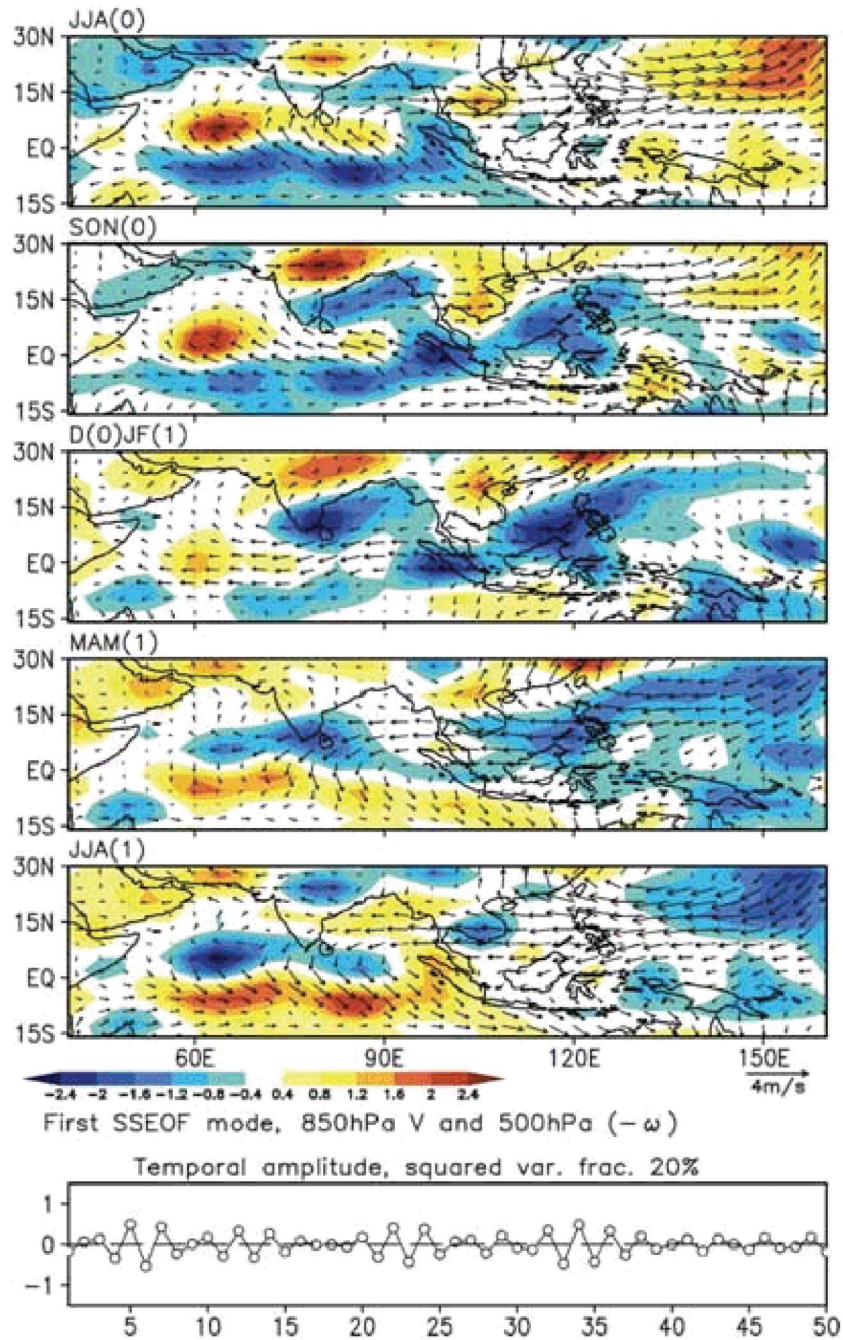


Plate 6. Seasonal evolution of 500 hPa vertical p velocity (color shaded, unit: Pa s^{-1}) and 850 hPa wind anomaly (vectors) associated with the TBO obtained from a SS-EOF analysis of 50 year output of the hybrid coupled GCM. The time coefficient of the SS-EOF mode is shown in the bottom plot. The vertical velocity has been multiplied by -1 so that positive contours represent enhanced convection anomalies.

SST in the IO in the preceding winter and spring, while no significant temperature changes are found over the Eurasian continent. At the 3–7 year window (Plate 4, right), a signif-

icant warming of the tropospheric mean temperature appears over the subtropical Eurasian continent in the preceding winter, with the correlation coefficient greater than

0.7. Meanwhile, a negative correlation center is located over the western equatorial IO. This north-south thermal contrast is even enhanced in northern spring and is significantly correlated with the summer monsoon rainfall. The physical processes that give rise to such a land-ocean thermal contrast are not clear, although several investigators [e.g., Meehl, 1997; Yang and Lau, 1998] have hypothesized that it might result from remote SST forcing in the tropics. The establishment of the meridional temperature gradient in the preceding season may help to set up the monsoon southwesterly wind earlier and stronger.

The time-filtering analysis above shows that the monsoon QB and LF modes have distinctive spatial and temporal structures. For the QB mode, a positive SSTA in the IO leads to a wet monsoon and the SSTA in the EP changes its phase in spring, whereas for the LF mode a cold SSTA in the EP persists from winter to summer and is associated with a wet monsoon.

The time-filtering analysis indicates that the Indian monsoon rainfall is significantly correlated with the IO SSTA in the preceding winter and spring on the TBO time scale. A natural question is, Through what process does the IO SSTA in the preceding seasons influence the monsoon? The IO SSTA may influence the Indian monsoon via both dynamic and thermodynamic effects. The dynamic impact is through induced upward motion in the monsoon sector that may compensate for the effect of El Niño forcing from the EP. The thermodynamic impact is through the moisture effect. We argue that a warm SSTA can increase local moisture over the ocean through enhanced surface evaporation. The overall increase of specific humidity over the

Indian Ocean is a good precondition for a strong monsoon, because after the monsoon onset the southwesterly flows would transport these excess moistures into the monsoon region. A strong monsoon enhances surface winds that cool the ocean through surface evaporation and ocean mixing, resulting in a colder than normal IO SSTA that further reduces the moisture accumulation and leads to a weak monsoon next year.

In addition to the IO SSTA, the low-level moisture convergence in the preceding spring is significantly correlated with the monsoon on the TBO time scale. The anomalous moisture convergence may influence the monsoon through the accumulation of local moisture. As we know, during the dry seasons the local atmosphere over India is in a convectively stable regime. Because of that, the convergent water vapor prior to the monsoon onset is used primarily for moistening the local air. The increase of local humidity may initially help strengthen the monsoon intensity, which may further induce anomalous southwesterly flows during the monsoon season and help to bring more moisture from the tropical ocean. Note that this anomalous moisture convergence mechanism differs from the effect of the IO SSTA. The former is associated with the moisture flux by anomalous winds, whereas the latter is related to anomalous moisture advection by the mean monsoon flow.

While the monsoon TBO is primarily controlled by local processes, the monsoon LF variability is attributed to the remote forcing of the SSTA in the Pacific. We argue that three possible processes may contribute to the rainfall anomaly on the lower-frequency time scale. The first is the direct impact of the EP SSTA through the vertical

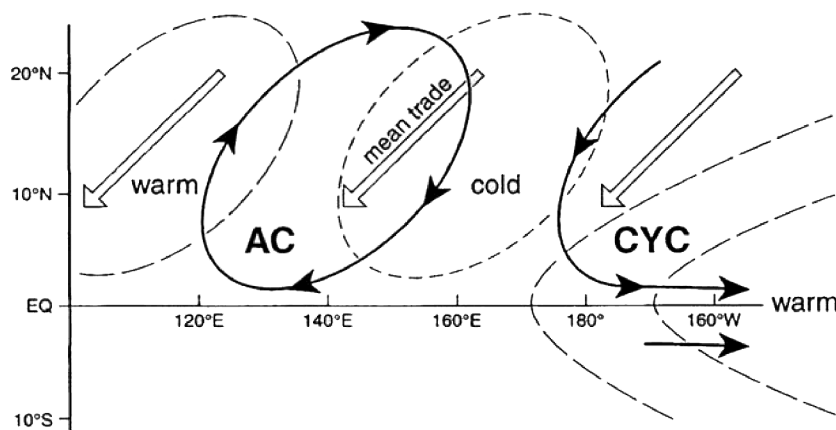


Figure 6. A schematic diagram illustrating the effect of a positive air-sea feedback between the PSAC and cold SSTA in WNP. The open arrow denotes the background mean trade wind, and heavy lines with black arrows represent the anomalous wind. The long (short) dashed lines represent a positive (negative) SSTA. From Wang *et al.* [2000].
© Copyright American Meteorological Society.

overturning of the large-scale east-west circulation [e.g., Meehl, 1987]. This mechanism can be readily seen from the wet-minus-dry composites of the velocity potential difference field (Figure 5). The second is the effect of the anomalous SST in the WP. Associated with a cold SSTA in the equatorial EP, a positive SSTA appears in the WP. This warm SSTA may further affect local convective activity and induce anomalous lower tropospheric cyclonic circulation off the Philippines [Tomita and Yasunari, 1993]. It is speculated that the enhanced convective activity in the WP may increase the frequency or intensity of the north-westward propagating synoptic-scale disturbances and thus enhance the monsoon trough from the equatorial WP to the Indian subcontinent. The third process is attributed to the impact of the remote tropical SSTA forcing on the midlatitude atmospheric circulation. The wet-minus-dry mean tropospheric temperature composite shows that 3–6 months prior to a wet monsoon a north-south thermal contrast has already been established across South Asia and the IO, with the warm core centered over the Tibetan Plateau (Plate 4, right). The location of this warm core is consistent with the hypotheses that Tibetan heating and/or Eurasian snow cover prior to the monsoon onset play an important role in the strength of the monsoon [e.g., Mooley and Shukla, 1987; Yanai et al., 1992]. This differs markedly from the monsoon TBO mode, in which the Indian subcontinent and the IO are both covered by an elongated warm anomaly belt in the preceding winter and spring. Thus, an enhanced (reduced) land-ocean thermal contrast precedes a strong (weak) monsoon on the lower-frequency time scale but not on the TBO time scale.

4. PACIFIC–EAST ASIA TELECONNECTION

What are the dominant seasonal evolving circulation patterns in the monsoon sector in association with the developing and decaying phases of ENSO? To answer the question, a season-sequence singular vector decomposition (SS-SVD) analysis method is applied [Wang et al., 2003b]. Plate 5 displays the evolution of anomalous 850 hPa winds and SST associated with ENSO turnabout revealed by the first SS-SVD mode. This mode describes 91% of the total covariance between the SST anomalies in the tropical Pacific and Indian oceans (40°E–90°W, 20°S–20°N) and five seasonal mean 850 hPa wind anomalies.

During the summer when the El Niño develops, the low-level circulation anomalies are dominated by an elongated anticyclonic ridge extending from the maritime continent to the southern tip of India. Associated with this anticyclonic ridge is a tilted belt of pronounced anomalous westerlies extending from the Bay of Bengal to the WNP, suppressed

convection over the maritime continent, and enhanced convection over the Philippine Sea (Plate 5a). The enhanced WNP monsoon trough greatly increases the number of tropical storm formations in the southeast quadrant of the tropical WNP (5°–17°N, 140°–170°E) [Chen et al., 1998; Wang and Chan, 2002]. On the other hand, the weak anticyclonic anomalies over India imply a moderately deficient IM.

During the fall of an El Niño–developing year, the southeastern IO (SEIO) anticyclone grows explosively, leading to a giant anticyclonic ridge dominating the IO with the anticyclone center at 10°S, 90°E, a titled ridge extending from western Australia all the way to the Arabian Sea (Plate 5b). Note that a new anomalous low-level anticyclone starts to form in the vicinity of Philippines.

In the mature phase of El Niño, D(0)/JF(1), the low-level circulation anomalies are dominated by two subtropical anticyclonic systems located in the SEIO and the WNP, respectively (Plate 5c). The former is a result of the weakening and eastward retreat of the SEIO anticyclone from boreal fall, while the later results from the amplification and eastward migration of the Philippine anticyclone. The most suppressed convection is centered east of the Philippine Sea.

MAM(1) and JJA(1) have similar anomaly patterns, which are characterized by the pronounced WNP anomalous anticyclone (Plates 5d and 5e). The intensity of the WNP anticyclone, however, decreases toward JJA(1). By summer JJA(1), subsidence controls the Philippine Sea and Southeast Asia, signifying weakening of the summer monsoon over the regions. The anomaly pattern exhibits nearly opposing polarities with that in the summer of the previous year, indicating a strong biennial tendency associated with the El Niño turnabout.

The most interesting feature of the seasonal evolving monsoon patterns in Plate 5 is the persistence of the anomalous anticyclone in the WNP from the El Niño peak winter to the subsequent summer. It is the anomalous anticyclone in JJA(1) that leads to enhanced rainfall in the Meiyu region through enhanced pressure gradients and moisture transport [Chang et al., 2000a, 2000b]. As the atmosphere itself does not hold a long memory, the persistence of the anomalous Philippine Sea anticyclone (PSAC) from the boreal winter to summer calls for a dynamic explanation.

The process through which ENSO has a delayed impact on the EAM was illustrated by Wang et al. [2000] (see a schematic diagram in Figure 6) and further confirmed by numerical experiments by Lau and Nath [2000]. The essential part of the proposed mechanism lies in a local positive air-sea feedback between atmospheric descending Rossby waves

and the underlying cold SST anomaly in the WNP that maintains the anomalous PSAC from the mature El Niño to the ensuing summer. This positive feedback, operating in the presence of background northeasterly trade winds, may be described as follows. To the east of the anomalous PSAC, the increased total wind speed cools the ocean surface where it induces excessive evaporation and entrainment. The cooling, in turn, suppresses convection and reduces latent heating in the atmosphere, which excites descending atmospheric Rossby waves that reinforce the PSAC in their decaying journey to the west. The initial triggering of the cold SSTA may be attributed to the atmospheric Rossby wave responses to the central equatorial Pacific heating during the El Niño peak winter; the so-induced anomalous flows coincide with

the background mean wind and lead to enhanced evaporation and thus the cooling of the local ocean surface. The initial triggering of an anomalous PSAC may arise from the cold surge intrusion from the Asian continent [Wang and Zhang, 2002; Lau and Nath, 2006] or the eastward propagation of a low-level anticyclone from the tropical IO [Chou, 2004; Chen *et al.*, 2007].

In contrast to its weakening in the El Niño decaying summer, the WNPM tends to strengthen in the El Niño developing summer (Plate 5a). The possible cause of this enhancement during the El Niño developing phase is as follows. First, it is attributed to the increases of low-level cyclonic vorticity associated with equatorial westerly anomalies [Wu *et al.*, 2009]. Second, in response to El Niño

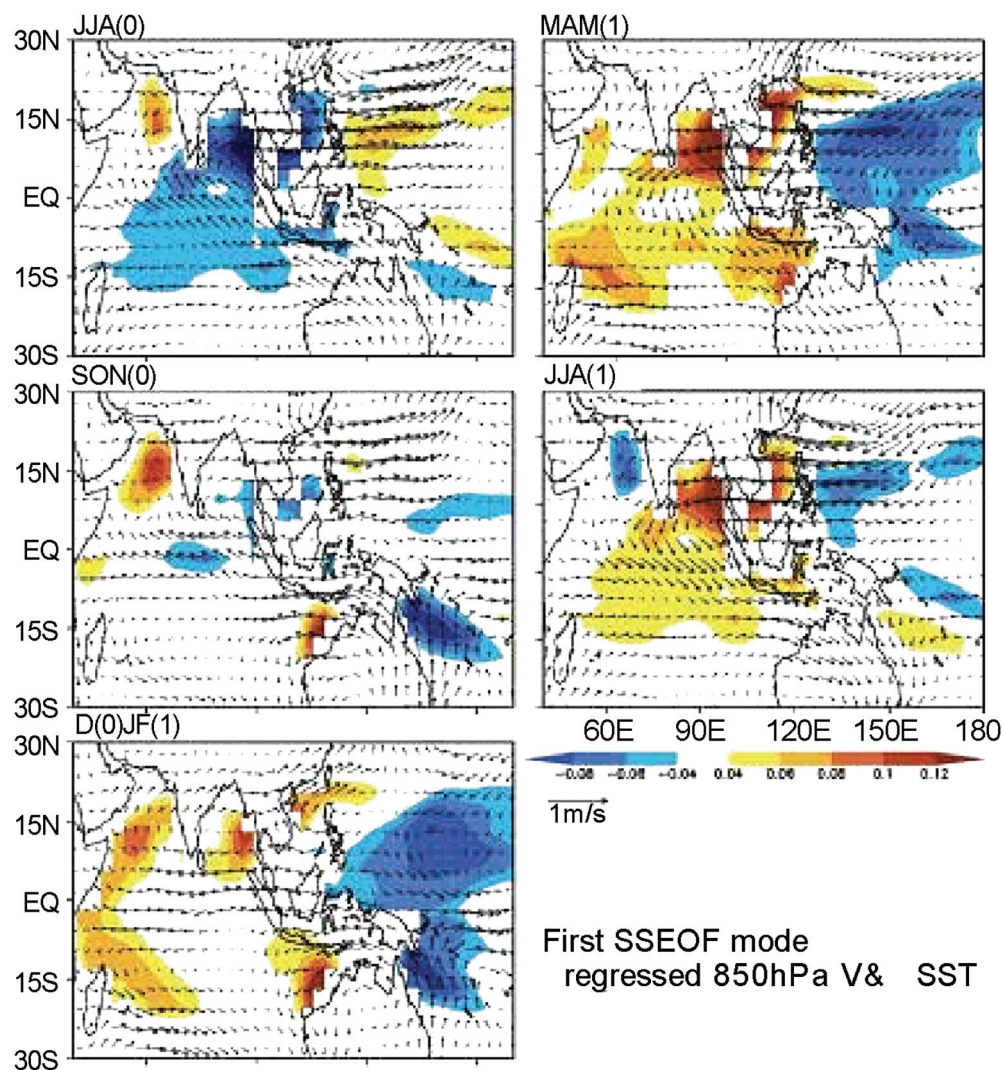


Plate 7. Same as Plate 6 except for the regressed SSTA (shading, unit: kelvin) field from the hybrid coupled GCM.

forcing, convection over the maritime continent is suppressed. The suppressed convection leads to an equatorial-asymmetric atmospheric Rossby wave response in the presence of the asymmetry of easterly shear of the summer mean zonal flow [Wang *et al.*, 2003b]. Thus, a strong anticyclonic cell appears north of the equator, with an anomalous ridge tilted northwestward toward the Indian subcontinent. This leads to dry monsoon over India. Meanwhile, the anomalous anticyclonic flow enhances low-level westerlies and thus convective activities over the WNP. This explains the observed negative correlation between the interannual anomalies of the IM and WNPM [Gu *et al.*, 2010].

5. TROPOSPHERIC BIENNIAL OSCILLATIONS IN THE INDO-PACIFIC WARM POOL

The tendency of the rainfall anomaly to “flip-flop” in successive years is referred to as the tropospheric biennial oscillation [Meehl, 1994, 1997]. Observations show that TBO is manifested over various monsoon regions such as Indonesia/northern Australia [Nicholls, 1978; Yasunari and Suppiah, 1988], East Asia/WNP [Lau and Sheu, 1988; Tian and Yasunari, 1992; Shen and Lau, 1995; Chang *et al.*, 2000a, 2000b; Wang and Li, 2004; Li and Wang, 2005],

and India [Mooley and Parthasarathy, 1984; Meehl, 1987; Rasmusson *et al.*, 1990; Yasunari, 1990, 1991].

Several theories have been proposed to understand the origin of the TBO (see Li *et al.* [2001b] for a review). Nicholls [1978] and Clarke *et al.* [1998] proposed that the TBO resulted from local air-sea interactions modulated by the annual cycle basic state. Meehl [1987] suggested that the southeastward propagation of anomalous convection might change the eastern Pacific SSTA in such a way that it altered the sign of the monsoon convection in the following year. Meehl [1997] further hypothesized a teleconnection mechanism through which anomalous tropical heating affects the midlatitude circulation and land temperatures. Chang and Li [2000] and Li *et al.* [2001c] demonstrated, in a coupled tropical atmosphere-ocean interaction model, that the TBO is an inherent monsoon mode, resulting from interactions among the Asian and Australian monsoons and tropical Indo-western Pacific oceans.

While recognizing the interactive nature of the monsoon and ENSO, it is essential to understand the fundamental cause of the TBO. So far there are two schools of thought. One is that the TBO is externally forced by the QB component of ENSO, as the delayed oscillator [Zebiak and Cane, 1987; Suarez and Schopf, 1988] may have an inherent

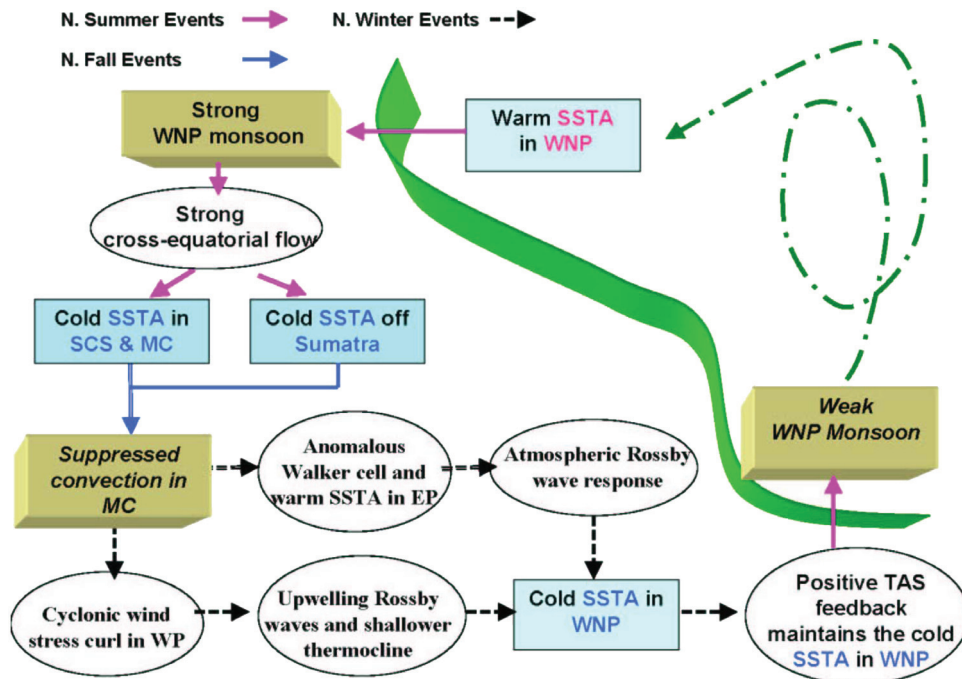


Plate 8. A schematic diagram illustrating essential processes that lead to the TBO in the tropical Pacific and Indian oceans. The left part of a green ribbon consists of a half of the TBO cycle, which starts from a strong WNP summer monsoon at year 0 and ends at a weak monsoon at year 1. The red, blue, and black arrows indicate northern summer, fall, and winter events, respectively.

biennial component. The other view is that the monsoon has an intrinsic biennial variability due to its interaction with adjacent warm oceans and the large-scale atmospheric circulation [e.g., *Chang and Li, 2000; Meehl and Arblaster, 2002a, 2002b*]. The latter view implies that the biennial component of the ENSO may arise from the remote teleconnection with the monsoon [*Kim and Lau, 2000; Chang and Li, 2001*].

To test the hypothesis that the ocean-atmosphere interactions in the monsoon/warm ocean region may lead to the TBO, *Li et al.* [2006] conducted idealized numerical experiments of a hybrid coupled atmosphere-ocean GCM in which the atmosphere and ocean are fully interactive only in the tropical IO and western Pacific. The atmospheric component of this hybrid coupled model is the ECHAM4 T30L19 version. The ECHAM4 has been coupled to an intermediate ocean model [*Wang et al., 1995*] without a heat flux correction [e.g., *Fu et al., 2002, 2003*]. The intermediate ocean model consists of two active layers of the upper ocean, a mixed layer with variable depth, and a thermocline layer overlying an inert deep ocean [*Wang et al., 1995*]. The latest version of the model combines the upper ocean dynamics described by *McCreary and Yu* [1992] and the mixed layer physics [*Gaspar, 1988*]. The model has a self-contained parameterization scheme for entrained water temperature that considers influences on entrained water temperature from both the thermocline displacement and the mixed layer temperature [*Wang et al., 1995*]. The effects of shear production, wind stirring, and buoyancy forcing are included in the vertical entrainment velocity calculation. The model has the capability of simulating realistic annual cycle and interannual variations of SST, thermocline depth, and mixed layer depth [*Fu and Wang, 2001*].

To explore the role of the atmosphere-warm ocean interaction, we designed an idealized hybrid coupled GCM experiment in which the atmosphere and ocean are coupled only in the tropical IO and western Pacific (30°S–30°N, 40°E–180°E), while the climatological monthly mean SST is specified elsewhere. By doing so, we exclude the effect of the remote El Niño forcing.

After the initial 10 year spin-up, the coupled model was integrated for 50 years. The long-term simulation shows that the coupled model is capable of simulating a realistic annual cycle and ENSO-like interannual variability in the equatorial Pacific. The seasonal mean SST errors are in general smaller than 1°C in most of the ocean domain except near the coast of North Africa in boreal summer and the coast of west Australia and the SCS in boreal winter.

The diagnosis of standard deviation of the total interannual (1–8 years) variability of the model SST and the relative strength of the QB (1.5–2.5 years) component

reveals that the greatest interannual SST variabilities appear in the BOB, SEIO, WNP, and South Pacific Convergence Zone, where the biennial component is also largest. The averaged ratio of the biennial SST variability in the four regions exceeds 60%, about a factor of 2 larger than the observed, indicating that in this model configuration without the eastern tropical Pacific, the TBO is a dominant signal. Strong TBO signals also appear in the midtropospheric (500 hPa) vertical motion and low-level (850 hPa) zonal and meridional wind components. The power spectra of the time series of the model SST and 500 hPa vertical velocity show that the TBO peaks, ranging from a period of 20–28 months, clearly appear in these spectra, and they exceed a 95% significance level. The results suggest that the monsoon-warm ocean interaction favors a pronounced biennial variability.

To illustrate the spatial pattern and evolutionary characteristics of the TBO in the Indo-Pacific warm ocean region, a season-sequence empirical orthogonal function (SS-EOF) analysis is performed for both the model and the NCEP reanalysis. Plate 6 illustrates the seasonal evolution of 850 hPa wind and 500 hPa vertical p velocity fields in the model. Here the vertical velocity has been multiplied by -1 so that a positive value in Plate 6 represents an enhanced rainfall anomaly. It is noted that the model in general captures the gross structure and evolution patterns of the observed TBO in the region. For instance, in JJA(0), the circulation anomaly in the SEIO is characterized by downward motion (or suppressed convection) and anticyclonic low-level flows, while in the WNP it is characterized by cyclonic flows and upward motion. The SEIO anticyclone is pronounced in the northern fall and decays in subsequent seasons. Subsidence motion and anticyclonic flows develop over the Philippines and SCS in SON(0), and they shift slightly eastward in subsequent seasons and persist until JJA(1). The circulation anomalies in JJA(1) have an opposite polarity relative to those in the previous summer.

Since the model does not contain the ENSO mode, the model TBO arises solely from air-sea interactions in the Indo-Pacific warm pool. What are specific processes that give rise to the TBO variability in this region? Plate 7 illustrates the seasonal evolution pattern of the SSTA, which is regressed on the basis of the time coefficient of the first SS-EOF mode. A significant surface cooling occurs in JJA(0) in the eastern IO and off the Asian coast, with maximum cold SSTA appearing in the BOB and SCS. While the cold SSTA decays in subsequent seasons, new cold SST anomalies develop in the western Pacific in SON(0) and DJF(1). In particular, the cold SSTA in the WNP reaches a peak in DJF(1) and persists for 2–3 seasons until the following summer, JJA(1), when the SSTA in the

eastern IO and SCS has completely reversed sign from a cold to a warm anomaly.

The diagnosis of the model SST budget reveals that the cooling in the IO in JJA(0) is primarily attributed to the surface evaporation and vertical ocean mixing because of enhanced surface wind speeds, whereas the cooling in the western Pacific in SON(0) and DJF(1) is mainly attributed to the ocean dynamic processes in response to anomalous wind stress curl (see discussions below). On the basis of the model circulation and SST evolution, a hypothesis is put forth to explain the TBO in the model. Assume that we start from a strong WNP monsoon in JJA(0). In response to enhanced WNP monsoon heating, northward low-level cross-equatorial winds are generated. The anomalous winds enhance the seasonal mean winds, leading to increased surface evaporation and ocean vertical mixing and thus negative SSTA in the eastern IO and off the Asian coast. It is seen from Plate 7 that the strongest SST cooling appears in the BOB, SCS, and maritime continent (MC). This SST cooling has a significant impact on the strength of the annual convective maximum that migrates to Southeast Asia in SON and to the MC in DJF [Meehl, 1987]. The so-induced suppressed convection in SCS and MC may further induce anomalous westerlies over the equatorial western Pacific through the atmospheric Kelvin wave response.

The curl of the zonal wind stress anomaly near the equator may exert a dynamic impact on SST by exciting upwelling oceanic Rossby waves and by lifting the ocean thermocline. As a result, the ocean surface cools. The diagnosis of the mixed layer heat budget in the ocean model confirmed that the negative SST tendency in the western Pacific in SON(0) and DJF(1) is indeed attributed to the ocean dynamics terms (i.e., 3-D ocean temperature advection), while the net heat flux effect is modest, particularly in DJF(1).

The cold SSTA over the WNP, once initiated by the ocean dynamics, may persist from northern winter to the following summer through the positive air-sea feedback proposed by Wang *et al.* [2000]. The persistent cold SSTA eventually leads to suppressed convection and thus a weaker WNPM in JJA(1), thus completing a TBO transition from a local cyclonic circulation in JJA(0) to an anticyclone in JJA(1). The weakened WNPM induces southward cross-equatorial flows, leading to anomalous ocean surface warming in the eastern IO and SCS, and thus, the second half of the TBO cycle begins in this region.

Plate 8 is a flowchart that summarizes the key physical processes implied from the hybrid coupled GCM experiments. Starting from a strong WNPM in boreal summer, the strong convection in the WNP causes strong northward cross-equatorial flows. The anomalous winds induce cold

SSTA in the SCS, MC, and SEIO off Sumatra, leading to suppressed convection in the MC through either a local SSTA impact on the seasonal convective maximum or its effect on surface wind divergence/moisture and local Walker circulation over the IO [Li *et al.*, 2002, 2003]. The suppressed convection in the MC induces anomalous westerlies in the western Pacific, which further leads to a cold SSTA in the WNP through either a direct ocean dynamic effect (via ocean Rossby waves and thermocline changes) or an indirect atmospheric effect (through the CP heating and associated atmospheric Rossby wave response). The so-induced cold SSTA in the WNP persists through the thermodynamic air-sea feedback and leads to the weakening of the WNP monsoon in the following summer. Thus, the second half cycle of the TBO begins. This confirms earlier hypotheses [e.g., Chang and Li, 2000; Li *et al.*, 2001c] that the biennial component of ENSO is a part of the TBO, resulting from teleconnections between the tropical Pacific and Indian oceans.

Note that the hybrid coupled GCM experiment above includes not only the atmosphere-ocean interaction but also the atmosphere-land interaction. To isolate the land effect, an additional (atmosphere-land-interaction-only) experiment was conducted by specifying the climatological monthly mean SST in the global oceans. The diagnosis of the model output, using the same SS-EOF analysis procedure, reveals that no observed TBO evolution patterns appear in this case, suggesting the importance of the atmosphere-warm ocean interaction in causing the observed TBO structure and evolution in the Indo-Pacific region.

6. CONCLUDING REMARKS

The spatial and temporal structures of the northward propagating boreal summer intraseasonal oscillation (BSISO) are revealed based on the analysis of both the ECHAM4 model simulation and the NCEP/NCAR reanalysis. The BSISO structure and evolution characteristics simulated by the model bear many similarities to those derived from the NCEP/NCAR reanalysis. The most notable features are remarkable meridional asymmetries, relative to the BSISO convection, in the vorticity and specific humidity fields. A positive vorticity perturbation with an equivalent barotropic structure appears a few latitude degrees north of the convection center. The maximum specific humidity also shows a clear northward shift in the lower troposphere.

Two internal atmospheric dynamics mechanisms are proposed to understand the cause of the northward propagation of the BSISO. The first is the vertical shear mechanism. The key process associated with this mechanism is the generation of the barotropic vorticity due to the coupling between

the free-atmosphere baroclinic and barotropic modes in the presence of the vertical shear of the mean flow. The induced barotropic vorticity in the free atmosphere further causes a moisture convergence in the PBL, leading to the northward shift of the convective heating. The second mechanism is the moisture-convection feedback mechanism. Two processes contribute to the northward shift of the low-level moisture. One is the moisture advection by the mean southerly wind in the PBL. Another is the moisture advection by the BSISO wind due to the mean meridional specific humidity gradient. The asymmetric specific humidity contributes further to the northward shift of the convective heating.

The spatial and temporal structures of atmospheric circulation and SST associated with the Indian monsoon rainfall variability on QB (2–3 years) and LF (3–7 years) time scales were investigated, using the domain-averaged Indian rainfall, the NCAR/NCEP reanalysis, and Reynolds SST data. We took both time-filtering and composite analysis approaches. The results indicate that physical processes that determine the monsoon rainfall variation on the 2–3 year and 3–7 year time scales are different. The QB variability of the monsoon is primarily determined by local processes in the IO. Both local SST and moisture flux convergence anomalies are highly correlated with the monsoon at a lagged time of 3–6 months. It is argued that a positive SSTA in the IO increases local moisture because of enhanced surface evaporation. The accumulation of these moistures leads to a strong monsoon through anomalous moisture advection by the summer mean flow.

The LF variability of the monsoon is primarily attributed to remote forcing mechanisms. Three possible processes may contribute to the monsoon variability on the 3–7 year time scale. The first is through the change of large-scale east-west circulation induced by the eastern Pacific SSTA. The second is attributed to the effect of the SSTA in the WNP through enhanced (or suppressed) convective activities along the monsoon trough region. The third is attributed to the tropical-midlatitude teleconnection: a strong north-south land-ocean thermal contrast occurs one to two seasons prior to a wet monsoon, and its persistence to boreal summer leads to the monsoon intensity change.

While the remote impact of ENSO on the Indian monsoon is primarily confined in the ENSO-developing summer, the El Niño has a delayed impact on the EAM during its decaying summer, even though the SSTA in the eastern equatorial Pacific has become normal. Such a delayed impact is primarily through a local positive air-sea feedback in the WNP that maintains the anomalous PSAC from the mature El Niño to the ensuing summer. This positive feedback depends crucially on the annual cycle of the background mean flow, and it is active only when the mean

northeasterly trade wind is present. Because of the positive feedback, the cold SSTA grows and persists in the WNP from boreal winter to late spring (until the monsoon onset) and thus has a significant impact on the WNPM and EAM in the subsequent summer. Recent studies [e.g., *Li et al.*, 2005; *Yang et al.*, 2007; *Wu et al.*, 2009] have suggested that El Niño-induced IO warming may have a remote impact on the WNPM in JJA(1).

The possible role of the monsoon–warm ocean interaction in generating TBO is investigated with a hybrid coupled GCM in which atmosphere and ocean are fully interactive only in the tropical western Pacific and Indian oceans, while in other regions a climatological SST is specified. A SS-EOF analysis approach is used to reveal the structure and seasonal evolution characteristics of the model TBO. It is noted that major convective activity centers associated with the TBO in the region reside in the southeastern Indian Ocean (SEIO) and WNP. Accompanying the TBO convection centers are two large-scale anticyclonic (or cyclonic) circulation patterns. The circulation anomalies have a first-baroclinic-mode vertical structure. The life cycle and evolution of the two anticyclonic (or cyclonic) flow anomalies in the SEIO and WNP are remarkably different. Whereas the anomaly in the SEIO is initiated in northern summer and reaches a peak phase in northern fall, the circulation anomaly in the WNP is initiated in northern fall and persists for 2–3 seasons until the subsequent summer and has a significant impact on the WNP summer monsoon.

The numerical experiment clearly demonstrates the importance of the warm ocean–atmosphere interaction in causing the TBO. The key processes involved include (1) cross-equatorial flows associated with the variability of the WNP monsoon, (2) impact of the local SSTA on the annual convective maximum over the SCS and MC and an associated regional-scale atmospheric circulation anomaly in the western equatorial Pacific, and (3) dynamic ocean response to the wind stress curl in the western Pacific. The coupled experiment above suggests that the teleconnection between the tropical IO and Pacific may lead to a TBO without the explicit involvement of the delayed oscillator dynamics. Both the Indian Ocean dipole and the biennial component of the ENSO are parts of the TBO [*Meehl et al.*, 2003].

A recent analysis of the Atmospheric Model Intercomparison Project (AMIP) models [*Zhou et al.*, 2009] showed that the SST-forced AMIP simulation reproduces the first two leading modes of the Asian-Australian monsoon rainfall variability with a skill that is comparable to the NCEP reanalysis in terms of the spatial patterns and the corresponding temporal variations, as well as their relationships with ENSO evolution. The skill of the AMIP simulation is seasonally dependent. DJF (JJA) has the highest (lowest) skill. The

multimodel ensemble result suggests the importance of local air-sea coupling effects over the monsoon domain.

In this chapter, we emphasize the Asian monsoon intra-seasonal and interannual variabilities. In reality, the monsoon also has significant variations in both shorter (such as synoptic and diurnal) and longer (interdecadal) time scales. While ENSO is the principle factor causing the monsoon interannual variation, it, nevertheless, can only explain a small fraction of the variability. The monsoon was found to have strong relationships with Eurasian circulation and north Pacific SST variability, which may or may not relate to ENSO [Lau, 2001]. The monsoon, while influenced by ENSO and other climate systems, may exert a strong impact on remote and local SSTA in the Pacific and Indian oceans [e.g., Matsumoto and Yamagata, 1991; Wainer and Webster, 1996; Chung and Nigam, 1999; Kim and Lau, 2000] and even in North America [Wang et al., 2001].

Acknowledgments. Discussions with Bin Wang, C.-P. Chang, and Jerry Meehl are greatly appreciated. This work was supported and by ONR grant N000140810256 and NRL grant N00173091G008 and by the International Pacific Research Center that is sponsored by the Japan Agency for Marine-Earth Science and Technology (JAMSTEC), NASA (NNX07AG53G), and NOAA (NA17RJ1230). This is SOEST contribution number 7880 and IPRC contribution number 665.

REFERENCES

- Barnett, T. P. (1991), The interaction of multiple time scales in the tropical climate system, *J. Clim.*, *4*, 269–285.
- Cadet, D. L. (1986), Fluctuations of precipitable water over the Indian Ocean, *Tellus, Ser. A*, *38*, 170–177.
- Chang, C.-P., and T. Li (2000), A theory for the tropical tropospheric biennial oscillation, *J. Atmos. Sci.*, *57*, 2209–2224.
- Chang, C.-P., and T. Li (2001), Nonlinear interactions between the TBO and ENSO, in *East Asian and Western Pacific Meteorology and Climate, World Sci. Ser. Meteorol. East Asia*, vol. 1, edited by C. P. Chang et al., pp. 167–179, World Sci., Singapore.
- Chang, C.-P., Y. Zhang, and T. Li (2000a), Interannual and interdecadal variations of the East Asian summer monsoon and tropical Pacific SSTs. Part I: Roles of the subtropical ridge, *J. Clim.*, *13*, 4310–4325.
- Chang, C.-P., Y. Zhang, and T. Li (2000b), Interannual and interdecadal variations of the East Asian summer monsoon and tropical Pacific SSTs. Part II: Meridional structure of the monsoon, *J. Clim.*, *13*, 4326–4340.
- Chang, C.-P., P. Harr, and J. Ju (2001), Possible roles of Atlantic circulations on the weakening Indian monsoon rainfall—ENSO relationship, *J. Clim.*, *14*, 2376–2380.
- Chen, G. T., and C.-P. Chang (1980), Structure and vorticity budget of early summer monsoon trough (Mei-Yu) over southeastern China and Japan, *Mon. Weather Rev.*, *108*, 942–953.
- Chen, J.-M., T. Li, and J. Shih (2007), Fall persistence barrier of SST in the South China Sea associated with ENSO, *J. Clim.*, *20*, 158–172.
- Chen, T.-C., S.-P. Weng, N. Yamazaki, and S. Kiehne (1998), Interannual variation in the tropical cyclone formation over the western North Pacific, *Mon. Weather Rev.*, *126*, 1080–1090.
- Chou, C. (2004), Establishment of the low-level wind anomalies over the western North Pacific during ENSO development, *J. Clim.*, *17*, 2195–2212.
- Chung, C., and S. Nigam (1999), Asian summer monsoon-ENSO feedback on the Cane-Zebiak model ENSO, *J. Clim.*, *12*, 2787–2807.
- Clarke, A. J., X. Liu, and S. van Gorder (1998), Dynamics of the biennial oscillation in the equatorial Indian and far western Pacific oceans, *J. Clim.*, *11*, 987–1001.
- Ding, Y. H. (1992), Summer monsoon rainfalls in China, *J. Meteorol. Soc. Jpn.*, *70*, 373–396.
- Ding, Y. H. (1994), *Monsoons Over China*, 420 pp., Springer, Dordrecht, Netherlands.
- Fu, X., and B. Wang (2001), A coupled modeling study of the annual cycle of Pacific cold tongue. Part I: Simulation and sensitivity experiments, *J. Clim.*, *14*, 765–779.
- Fu, X., B. Wang, and T. Li (2002), Impacts of air-sea coupling on the simulation of the mean Asian summer monsoon in the ECHAM4 model, *Mon. Weather Rev.*, *130*, 2889–2904.
- Fu, X., B. Wang, T. Li, and J. McCreary (2003), Coupling between northward propagating ISO and SST in the Indian Ocean, *J. Atmos. Sci.*, *60*, 1733–1753.
- Gaspar, P. (1988), Modeling the seasonal cycle of the upper ocean, *J. Phys. Oceanogr.*, *18*, 161–180.
- Gu, D., T. Li, Z. Ji, and B. Zheng (2010), On the western North Pacific monsoon, Indian monsoon and Australian monsoon phase relations, *J. Clim.*, in press.
- Jiang, X., T. Li, and B. Wang (2004), Structures and mechanisms of the northward propagating boreal summer intraseasonal oscillation, *J. Clim.*, *17*, 1022–1039.
- Johnson, R. H., Z. Wang, and J. F. Bresch (1993), Heat and moisture budgets over China during the early summer monsoon, *J. Meteorol. Soc. Jpn.*, *71*, 137–152.
- Ju, J., and J. M. Slingo (1995), The Asian summer monsoon and ENSO, *Q. J. R. Meteorol. Soc.*, *121*, 1133–1168.
- Kawamura, R. (1998), A possible mechanism of the Asian summer monsoon-ENSO coupling, *J. Meteorol. Soc. Jpn.*, *76*, 1009–1027.
- Kemball-Cook, S. R., and B. Wang (2001), Equatorial waves and air-sea interaction in the boreal summer intraseasonal oscillation, *J. Clim.*, *14*, 2923–2942.
- Kim, K.-M., and K.-M. Lau (2000), Dynamics of monsoon-induced biennial variability in ENSO, *Geophys. Res. Lett.*, *28*, 315–318.
- Krishnamurti, T. N., and D. Subrahmanyam (1982), The 30–50 day mode at 850 mb during MONEX, *J. Atmos. Sci.*, *39*, 2088–2095.

- Kumar, K. K., B. Rajagopalan, and M. C. Cane (1999), On the weakening relationship between the Indian monsoon and ENSO, *Science*, *284*, 2156–2159.
- Lau, K. M. (2001), Monsoon-ENSO relationship: A new paradigm, in *Dynamics of Atmospheric and Oceanic Circulations and Climate*, edited by M. Wang et al., pp. 533–551, China Meteorol. Press, Beijing.
- Lau, K.-M., and P. H. Chan (1986), Aspects of the 40–50 day oscillation during the northern summer as inferred from outgoing longwave radiation, *Mon. Weather Rev.*, *114*, 1354–1367.
- Lau, K.-M., and P. J. Sheu (1988), Annual cycle, quasi-biennial oscillation, and Southern Oscillation in global precipitation, *J. Geophys. Res.*, *93*, 10,975–10,988.
- Lau, K.-M., and H. T. Wu (2001), Principal modes of rainfall–SST variability of the Asian summer monsoon: A reassessment of the monsoon–ENSO relationship, *J. Clim.*, *14*, 2880–2895.
- Lau, K.-M., and S. Yang (1996), The Asian monsoon and predictability of the tropical ocean-atmosphere system, *Q. J. R. Meteorol. Soc.*, *122*, 945–957.
- Lau, K.-M., G. J. Yang, and S. Shen (1988), Seasonal and intraseasonal climatology of summer monsoon rainfall over East Asia, *Mon. Weather Rev.*, *116*, 18–37.
- Lau, N.-C., and M. J. Nath (2000), Impacts of ENSO on the variability of the Asian-Australian monsoons as simulated in GCM experiments, *J. Clim.*, *13*, 4287–4309.
- Lau, N.-C., and M. J. Nath (2006), ENSO modulation of the interannual and intraseasonal variability of the East Asian monsoon—A model study, *J. Clim.*, *19*, 4508–4530.
- Lawrence, D. M., and P. J. Webster (2002), The boreal summer intraseasonal oscillation: Relationship between northward and eastward movement of convection, *J. Atmos. Sci.*, *59*, 1593–1606.
- Li, C., and M. Yanai (1996), The onset and interannual variability of the Asian summer monsoon in relation to land-sea thermal contrast, *J. Clim.*, *9*, 358–375.
- Li, T., and B. Wang (1994), The influence of sea surface temperature on the tropical intraseasonal oscillation: A numerical experiment, *Mon. Weather Rev.*, *122*, 2349–2362.
- Li, T., and B. Wang (2005), A review on the western North Pacific monsoon: Synoptic-to-interannual variabilities, *Terr. Atmos. Oceanic Sci.*, *16*, 285–314.
- Li, T., and Y. Zhang (2002), Processes that determine the quasi-biennial and lower-frequency variability of the South Asian monsoon, *J. Meteorol. Soc. Jpn.*, *80*, 1149–1163.
- Li, T., Y. Zhang, C.-P. Chang, and B. Wang (2001a), On the relationship between Indian Ocean SST and Asian summer monsoon, *Geophys. Res. Lett.*, *28*, 2843–2846.
- Li, T., B. Wang, and C.-P. Chang (2001b), Theories on the tropospheric biennial oscillation: A review, in *Dynamics of Atmospheric and Oceanic Circulations and Climate*, edited by M. Wang et al., pp. 252–276, China Meteorol. Press, Beijing.
- Li, T., C.-W. Tham, and C.-P. Chang (2001c), A coupled air-sea-monsoon oscillator for the tropospheric biennial oscillation, *J. Clim.*, *14*, 752–764.
- Li, T., Y. Zhang, E. Lu, and D. Wang (2002), Relative role of dynamic and thermodynamic processes in the development of the Indian Ocean dipole: An OGCM diagnosis, *Geophys. Res. Lett.*, *29*(23), 2110, doi:10.1029/2002GL015789.
- Li, T., B. Wang, C.-P. Chang, and Y. Zhang (2003), A theory for the Indian Ocean dipole-zonal mode, *J. Atmos. Sci.*, *60*, 2119–2135.
- Li, T., Y.-C. Tung, and J.-W. Hwu (2005), Remote and local SST forcing in shaping Asian-Australian monsoon anomalies, *J. Meteorol. Soc. Jpn.*, *83*, 153–167.
- Li, T., P. Liu, X. Fu, B. Wang, and G. A. Meehl (2006), Temporal structures and mechanisms of the tropospheric biennial oscillation in the Indo-Pacific warm ocean regions, *J. Clim.*, *19*, 3070–3087.
- Lorenc, A. C. (1984), The evolution of planetary-scale 200 mb divergent flow during the FGGE year, *Q. J. R. Meteorol. Soc.*, *120*, 427–441.
- Madden, R. A., and P. R. Julian (1971), Detection of a 40-50 day oscillation in the zonal wind in the tropical Pacific, *J. Atmos. Sci.*, *28*, 702–708.
- Madden, R. A., and P. R. Julian (1972), Description of global-scale circulation cells in the tropics with a 40–50 day period, *J. Atmos. Sci.*, *29*, 1109–1123.
- Matsumoto, Y., and T. Yamagata (1991), On the origin of a model ENSO in the western Pacific, *J. Meteorol. Soc. Jpn.*, *69*, 197–207.
- McCreary, J. P., and Z. J. Yu (1992), Equatorial dynamics in a 2.5-layer model, *Prog. Oceanogr.*, *29*, 61–132.
- Meehl, G. A. (1987), The annual cycle and interannual variability in the tropical Pacific and Indian Ocean regions, *Mon. Weather Rev.*, *115*, 27–50.
- Meehl, G. A. (1994), Coupled land-ocean-atmosphere processes and south Asian monsoon variability, *Science*, *266*, 263–267.
- Meehl, G. A. (1997), The South Asian monsoon and the tropospheric biennial oscillation, *J. Clim.*, *10*, 1921–1943.
- Meehl, G. A., and J. M. Arblaster (2002a), The tropospheric biennial oscillation and Asian-Australian monsoon rainfall, *J. Clim.*, *15*, 722–744.
- Meehl, G. A., and J. M. Arblaster (2002b), GCM sensitivity experiments for the Indian monsoon and tropospheric biennial oscillation transition conditions, *J. Clim.*, *15*, 923–944.
- Meehl, G. A., J. M. Arblaster, and J. Loschnigg (2003), Coupled ocean-atmosphere dynamical processes in the tropical Indian and Pacific Ocean regions and the TBO, *J. Clim.*, *16*, 2138–2158.
- Mooley, D. A., and B. Parthasarathy (1984), Fluctuations in all-India summer monsoon rainfall during 1871–1978, *Clim. Change*, *6*, 287–301.
- Mooley, D. A., and J. Shukla (1987), Variability and forecasting of the summer monsoon rainfall over India, in *Monsoon Meteorology*, edited by C.-P. Chang and T. N. Krishnamurti, pp. 26–59, Oxford Univ. Press, New York.
- Murakami, M. (1979), Large-scale aspects of deep convective activity over the GATE data, *Mon. Weather Rev.*, *107*, 994–1013.

- Murakami, T., T. Nakazawa, and J. He (1984), On the 40-50 day oscillations during the 1979 Northern Hemisphere summer. I: Phase propagation, *J. Meteorol. Soc. Jpn.*, *62*, 440–468.
- Nicholls, N. (1978), Air-sea interaction and the quasi-biennial oscillation, *Mon. Weather Rev.*, *106*, 1505–1508.
- Nordeng, T. E. (1996), Extended versions of the convective parameterization scheme at ECMWF and their impact on the mean and transient activity of the model in the tropics, *ECMWF Res. Dep. Tech. Memo.* *206*, 41 pp., Eur. Cent. for Medium-Range Weather Forecasts, Reading, U. K.
- Rasmusson, E. M., and T. H. Carpenter (1983), The relationship between eastern equatorial Pacific sea surface temperatures and rainfall over India and Sri Lanka, *Mon. Weather Rev.*, *111*, 517–528.
- Rasmusson, E. M., X.-L. Wang, and C. F. Ropelewski (1990), The biennial component of ENSO variability, *J. Mar. Syst.*, *1*, 71–96.
- Reynolds, R. W., and T. M. Smith (1994), Improved global sea surface temperature analyses using optimum interpolation, *J. Clim.*, *7*, 929–948.
- Roeckner, E., K. Arpe, L. Bengtsson, M. Christoph, M. Claussen, L. Dmenil, M. Esch, M. Giorgetta, U. Schlese, and U. Schulzweida (1996), The atmospheric general circulation model ECHAM-4: Model description and simulation of present-day climate, *Rep.* *218*, 90 pp., Max-Planck-Inst. für Meteorol., Hamburg, Germany.
- Shen, S., and K.-M. Lau (1995), Biennial oscillation associated with the East Asian summer monsoon and tropical Pacific sea surface temperatures, *J. Meteorol. Soc. Jpn.*, *73*, 105–124.
- Sikka, D. R., and S. Gadgil (1980), On the maximum cloud zone and the ITCZ over Indian longitudes during the southwest monsoon, *Mon. Weather Rev.*, *108*, 1840–1853.
- Suarez, M. J., and P. S. Schopf (1988), A delayed action oscillator for ENSO, *J. Atmos. Sci.*, *45*, 3283–3287.
- Tanaka, M. (1997), Interannual and interdecadal variations of the western North Pacific monsoon and the East Asian Baiu rainfall and their relationship to ENSO cycles, *J. Meteorol. Soc. Jpn.*, *75*, 1109–1123.
- Tao, S. Y. and L. X. Chen (1987), A review of recent research of the East Asian summer monsoon in China, in *Monsoon Meteorology*, edited by C.-P. Chang and T. N. Krishnamurti, pp. 60–92, Oxford Univ. Press, New York.
- Tian, S. F., and T. Yasunari (1992), Time and space structure of interannual variations in summer rainfall over China, *J. Meteorol. Soc. Jpn.*, *70*, 585–596.
- Tiedtke, M. (1989), A comprehensive mass flux scheme for cumulus parameterization in large-scale models, *Mon. Weather Rev.*, *117*, 1779–1800.
- Tomita, T., and T. Yasunari (1993), The two types of ENSO, *J. Meteorol. Soc. Jpn.*, *71*, 273–284.
- Tomita, T., and T. Yasunari (1996), Role of the northeast winter monsoon on the biennial oscillation of the ENSO/monsoon system, *J. Meteorol. Soc. Jpn.*, *74*, 399–413.
- Wainer, I., and P. J. Webster (1996), Monsoon-ENSO interaction using a simple coupled ocean-atmosphere model, *J. Geophys. Res.*, *101*, 25,599–25,614.
- Waliser, D. E., et al. (2003), AGCM simulations of intraseasonal variability associated with the Asian summer monsoon, *Clim. Dyn.*, *21*, 423–446.
- Walker, G. T. (1923), Correlations in seasonal variations of weather. VIII, A further study of world weather, *Mem. Indian Meteorol. Dep.*, *24*, 75–131.
- Walker, G. T. (1924), Correlations in seasonal variations of weather. VIII, A further study of world weather, *Mem. Indian Meteorol. Dep.*, *24*, 275–332.
- Wang, B., and J. C.-L. Chan (2002), How strong ENSO regulates tropical storm activity over the western North Pacific, *J. Clim.*, *15*, 1643–1658.
- Wang, B., and T. Li (1993), A simple tropical atmospheric model of relevance to short-term climate variation, *J. Atmos. Sci.*, *50*, 260–284.
- Wang, B., and T. Li (1994), Convective interaction with boundary-layer dynamics in the development of a tropical intraseasonal system, *J. Atmos. Sci.*, *51*, 1386–1400.
- Wang, B., and T. Li (2004), East Asian monsoon-ENSO interactions, in *East Asian and Western Pacific Meteorology and Climate*, *World Sci. Ser. Meteorol. East Asia*, vol. 2, edited by C. P. Chang et al., pp. 177–212, World Sci., Singapore.
- Wang, B., and H. Lin (2002), Rainy seasons of the Asian-Pacific monsoon, *J. Clim.*, *15*, 386–398.
- Wang, B., and H. Rui (1990), Synoptic climatology of transient tropical intraseasonal convection anomalies: 1975–1985, *Meteorol. Atmos. Phys.*, *44*, 43–61.
- Wang, B., and R. Wu (1997), Peculiar temporal structure of the South China Sea summer monsoon, *Adv. Atmos. Sci.*, *14*, 177–194.
- Wang, B., and X. Xie (1997), A model for the boreal summer intraseasonal oscillation, *J. Atmos. Sci.*, *54*, 72–86.
- Wang, B., and Q. Zhang (2002), Pacific–East Asian teleconnection, Part II: How the Philippine Sea anticyclone is established during El Niño development, *J. Clim.*, *15*, 3252–3265.
- Wang, B., T. Li, and P. Chang (1995), An intermediate model of the tropical Pacific ocean, *J. Phys. Oceanogr.*, *25*, 1599–1616.
- Wang, B., R. Wu, and X. Fu (2000), Pacific–East Asian teleconnection: How does ENSO affect East Asian climate?, *J. Clim.*, *13*, 1517–1536.
- Wang, B., R. Wu, and K.-M. Lau (2001), Interannual variability of the Asian summer monsoon: Contrasts between the Indian and the western North Pacific–East Asian monsoons, *J. Clim.*, *14*, 4073–4090.
- Wang, B., S. C. Clemons, and P. Liu (2003a), Contrasting the Indian and East Asian monsoons: Implications on geologic timescales, *Mar. Geol.*, *201*(1–3), 5–21.
- Wang, B., R. Wu, and T. Li (2003b), Atmosphere–warm ocean interaction and its impacts on Asian–Australian monsoon variation, *J. Clim.*, *16*, 1195–1211.
- Webster, P. J. (1983), Mechanisms of low-frequency variability: Surface hydrological effects, *J. Atmos. Sci.*, *40*, 2110–2124.
- Webster, P. J., and S. Yang (1992), Monsoon and ENSO: Selectively interactive systems, *Q. J. R. Meteorol. Soc.*, *118*, 877–926.

- Webster, P. J., V. O. Magana, T. N. Palmer, J. Shukla, R. A. Tomas, M. Yanai, and T. Yasunari (1998), Monsoons: Processes, predictability, and the prospects for prediction, *J. Geophys. Res.*, *103*, 14,451–14,510.
- Wu, B., T. Zhou, and T. Li (2009), Seasonally evolving dominant interannual variability modes of East Asian climate, *J. Clim.*, *22*, 2992–3005.
- Wu, R., and B. Wang (2001), Multi-stage onset of the summer monsoon over the western North Pacific, *Clim. Dyn.*, *17*, 277–289.
- Xie, A., Y.-S. Chung, X. Liu, and Q. Ye (1998), The interannual variations of the summer monsoon onset over the South China Sea, *Theor. Appl. Climatol.*, *59*(4), 201–213.
- Xie, P., and P. A. Arkin (1997), Global precipitation: A 17-year monthly analysis based on gauge observations, satellite estimates and numerical model outputs, *Bull. Am. Meteorol. Soc.*, *78*, 2539–2558.
- Yanai, M., C. Li, and Z. Song (1992), Seasonal heating of the Tibetan Plateau and its effects on the evolution of the Asian summer monsoon, *J. Meteorol. Soc. Jpn.*, *70*, 319–351.
- Yang, J., Q. Liu, S.-P. Xie, Z. Liu, and L. Wu (2007), Impact of the Indian Ocean SST basin mode on the Asian summer monsoon, *Geophys. Res. Lett.*, *34*, L02708, doi:10.1029/2006GL028571.
- Yang, S., and K.-M. Lau (1998), Influences of sea surface temperature and ground wetness on Asian summer monsoon, *J. Clim.*, *11*, 3230–3246.
- Yang, S., K.-M. Lau, and M. Sankar-Rao (1996), Precursory signals associated with the interannual variability of the Asian summer monsoon, *J. Clim.*, *9*, 949–964.
- Yasunari, T. (1979), Cloudiness fluctuations associated with the Northern Hemisphere summer monsoon, *J. Meteorol. Soc. Jpn.*, *57*, 227–242.
- Yasunari, T. (1980), A quasi-stationary appearance of 30- to 40-day period in the cloudiness fluctuations during the summer monsoon over India, *J. Meteorol. Soc. Jpn.*, *58*, 225–229.
- Yasunari, T. (1990), Impact of the Indian monsoon on the coupled atmosphere/ocean system in the tropical Pacific, *Meteorol. Atmos. Phys.*, *44*, 29–41.
- Yasunari, T. (1991), The monsoon year—A new concept of the climatic year in the tropics, *Bull. Am. Meteorol. Soc.*, *72*, 1331–1338.
- Yasunari, T., and R. Suppiah (1988), Some problems on the interannual variability of Indonesian monsoon rainfall, in *Tropical Rainfall Measurements*, edited by J. S. Theon and N. Fugono, pp. 113–122, A. Deepak, Hampton, Va.
- Yeh, D.-Z., and R.-H. Huang (1996), *Study on the Regularity and Formation Reason of Drought and Flood in the Yangtze and Huaihe River Regions* (in Chinese), 387 pp., Shandong Sci. and Technol., Jinan, China.
- Zebiak, S. E., and M. A. Cane (1987), A model El Niño–Southern Oscillation, *Mon. Weather Rev.*, *115*, 2262–2278.
- Zhang, R., A. Sumi, and M. Kimoto (1996), Impact of El Niño on the East Asian monsoon: A diagnostic study of the '86/87 and '91/92 events, *J. Meteorol. Soc. Jpn.*, *74*, 49–62.
- Zhou, T., L. Zhang, and H. Li (2008), Changes in global land monsoon area and total rainfall accumulation over the last half century, *Geophys. Res. Lett.*, *35*, L16707, doi:10.1029/2008GL034881.
- Zhou, T., B. Wu, and B. Wang (2009), How well do atmospheric general circulation models capture the leading modes of the interannual variability of Asian-Australian monsoon?, *J. Clim.*, *22*, 1159–1173.
- Zhou, T.-J., and R.-C. Yu (2005), Atmospheric water vapor transport associated with typical anomalous summer rainfall patterns in China, *J. Geophys. Res.*, *110*, D08104, doi:10.1029/2004JD005413.
- Zhu, Q., J. He, and P. Wang (1986), A study of circulation differences between East-Asian and Indian summer monsoons with their interaction, *Adv. Atmos. Sci.*, *3*, 466–477.

Li, T., Department of Meteorology, University of Hawai'i at Mānoa, 2525 Correa Road, Honolulu, HI 96822, USA. (timli@hawaii.edu)

